Applied Catalysis B: Environmental 327 (2023) 122465

Contents lists available at ScienceDirect

Applied Catalysis B: Environmental

journal homepage: www.elsevier.com/locate/apcatb

First PEM photoelectrolyser for the simultaneous selective glycerol valorization into value-added chemicals and hydrogen generation

Jie Yu, Jesús González-Cobos *, Frederic Dappozze, Nicolas Grimaldos-Osorio, Philippe Vernoux, Angel Caravaca *, Chantal Guillard *

Univ Lyon, Université Claude Bernard Lyon 1, CNRS, IRCELYON, F-69626 Villeurbanne, France

ARTICLE INFO

Keywords:
Photoelectrocatalysis
Polymer electrolyte membrane
Glycerol
Electrolysis
Hydrogen

ABSTRACT

The photoelectrocatalytic (PEC) valorization of glycerol is emerging for the co-generation of hydrogen and value-added organics like glyceraldehyde (GAD) or dihydroxyacetone (DHA). In this work, we have designed, tested and optimized a pioneering photoelectrolyser with a non-noble metal-based photoanode (WO_3), operating in near-neutral conditions and using a proton-exchange membrane (PEM) which ensures the elution of a purified hydrogen stream from the cathode side while selectively oxidizing glycerol on the anode. The influence of light irradiation, external bias and cell temperature has been investigated, leading to GAD and DHA production rates of 11.1 and 5.2 mmol m^{-2} h^{-1} at 60 ºC and 1.2 V, along with 44.0 mmol H_2 m^{-2} h^{-1}. The long-term stability of the photoelectrolyser has also been validated and the particularities of this system with respect to other conventional devices have been discussed. PEC stands as a promising sustainable technology for the simultaneous H_2 generation and biomass valorization.

1. Introduction

Glycerol is an important by-product (~2.2 Mt worldwide in 2019 [1]) of the production of biodiesel as an alternative to fossil fuels and of soap manufacture. Being largely available and cheap, its valorization is not only encouraged for the global consensus on carbon neutralization, but also highly economically profitable. This is especially relevant when dealing with the selective production of its primary 3 C oxidation products, glyceraldehyde (GAD) and dihydroxyacetone (DHA), which are key precursors in the synthesis of cosmetics, polymers and biodegradable emulsifiers [2–6]. Besides, green hydrogen is regarded as one of the most important energy carriers for global energy transformation and development, given its high gravimetric energy density and its potential environmentally friendly implementation [7,8]. In this sense, a promising pathway for simultaneous glycerol valorization into value-added chemicals and pure green hydrogen is the photoelectrocatalysis (PEC) using renewable energy sources. This technology is more efficient than photocatalysis (PC) because external voltage can promote the separation of photogenerated electrons and holes. Therefore, PEC has gradually attracted the attention of academia and industry in recent years [9–11].

Glycerol-upgrading by PEC process is composed of two half-reactions: glycerol electrooxidation/oxygen evolution reaction (OER) at the anodic catalyst, and hydrogen evolution reaction (HER) at the cathodic catalyst. Despite recent several achievements, four main bottlenecks need to be addressed:

There is insufficient attention on both half-reactions simultaneously, i.e., glycerol oxidation and hydrogen evolution. Many studies are focused only on the cathodic hydrogen production and the anodic reactions are to some extent ignored. The products of the glycerol electrooxidation have not been analyzed in some cases [12–17] and, when they have been, the reaction has not always resulted in the production of the desired primary products. For example, in some cases, the selectively obtained product is glycerate [18–20], glycolate [20,21], lactate [20] or formate [22–25].

The utilization of precious metals like Pt [20,26–29], Au [30–32] and Pd [33–35], either as main active phase or as co-catalyst, decreases the PC and PEC economic competitiveness. In particular, in this work, the concern of replacing the noble metals has been focused on the anodic catalyst.

* Corresponding authors.
E-mail addresses: jesus.gonzalez-cobos@ircelyon.univ-lyon1.fr (J. González-Cobos), angel.caravaca@ircelyon.univ-lyon1.fr (A. Caravaca), chantal.guillard@ircelyon.univ-lyon1.fr (C. Guillard).

https://doi.org/10.1016/j.apcatb.2023.122465
Received 25 November 2022; Received in revised form 19 January 2023; Accepted 11 February 2023
Available online 13 February 2023

Most of the studies are carried out under harsh reaction conditions, i.e., using acid (e.g., H_2SO_4) [24,36–38] or alkaline concentrated solutions (e.g., KOH, NaOH) [18–22] as electrolytes, increasing the safety risks of storage and transportation and environmental hazards in large-scale production. For instance, Wang et al. proposed a CoNiFe-LDHs-decorated Ta_3N_5 nanotube array for the simultaneous generation of anodic formate and cathodic hydrogen in a 1.0 M NaOH electrolyte, [22] while the highest DHA selectivities (above 50%) have been reached by using solutions with pH = 2 [24,36–38]. There are very few PEC works performed under neutral or near-neutral conditions [24,25,39,40] and only two of them achieved the selective generation of $C_{3\ s}$, by Gu et al. [39] and by this group [40]. In both cases, WO_3-based anodes showed to be excellent materials for the selective glycerol oxidation, with selectivities up to c.a. 90% for GAD+DHA.

Apart from the unavoidable purification concerns of anodic liquid products (their separation from the liquid electrolyte), the generation of pure H_2 stream from glycerol electrolysis/photoelectrolysis is not ensured in the traditional 3-electrode PEC cells, unless there is a complete absence of any other gaseous products derived from the anode (e.g., CO or CO_2 from undesired glycerol oxidation reactions under neutral or acid conditions, or O_2 from the competitive water oxidation reaction at high enough potentials) [41,42]. Furthermore, the non-separation of the anodic and cathodic compartments may lead to side reduction reactions or poisoning phenomena at the cathode due to adsorbed organics adsorption. This is the case of the above-mentioned works, where both anodic and cathodic half-reactions took place in the same gas/liquid compartment. In view to its practical application, this configuration may increase the process complexity and economical cost due to the need for hypothetical products post-purification operations.

Polymer electrolyte membrane (PEM) cells using a thin solid electrolyte membrane to separate anode and cathode electrodes show several advantages with respect to liquid electrolyte cells, such as the separation of any possible gaseous oxidation products from the cathodic hydrogen effluent, typically lower ohmic resistance, higher compactness and better fluid dynamics, which lead to improved durability and efficiency [43,44]. PEM cells have been widely used in the field of electrocatalytic hydrogen generation from alcohols [45–50]. In particular, glycerol electrolysis was studied in PEM configuration with a proton-conducting membrane by Kim et al. [51], Marshall and Haverkamp [52], and Fan et al. [53]. There are also several works using an anion-exchange membrane, from the groups of Linares [54,55], Vizza [56] and Schuhmann [57–59]. However, the employed anodes were found to mainly produce glycerate [51,54–56], tartronate [54–56,58] or formate [53,57–59]. Therefore, to the best of our knowledge, the present study is the first one that simultaneously investigates the production of hydrogen and the selective glycerol valorization to GAD or DHA in a PEM cell, for either glycerol electrolysis or photoelectrolysis. Furthermore, the photoelectrocatalytic route is also herein explored, for the first time, to boost the glycerol selective oxidation in a PEM configuration. To date, there are very few studies in literature employing compact PEM cell configurations under PEC conditions and they were used for water splitting at room temperature, either in liquid-phase [60–63] or in gas-phase [63–65]. Thus, the application of the PEC approach to glycerol electrolysis in a PEM device is totally innovative.

In this work, a PEM Photoelectrolyser was designed to perform the separated glycerol oxidation to high value-added products in the anode compartment, together with the simultaneous green H_2 generation in the cathodic compartment. Monoclinic WO_3 synthesized by a simple hydrothermal method with proper crystallinity, acidity and redox properties (oxygen vacancies due to a ratio of W^{5+}/W^{6+} of ~18%/82%) was selected as the photoanode electrode due to its high selectivity towards GAD under near-neutral pH conditions observed in our previous work [40]. The operation parameters of this cell have been optimized, focusing not only on the applied potential but also on the cell temperature. This latter key parameter could significantly affect the reaction kinetics, mass transfer and photo- or electro-induced charge separation rate, but has been only scarcely studied in a three-electrode cell configuration. For this purpose, the bifunctional PEM system, dedicated not only to the anodic glycerol selective oxidation but also to the cathodic green energy H_2 generation, has been studied under (thermo) catalytic (TC), photocatalytic (PC), electrocatalytic (EC) and combined PEC conditions. The performance of the system has been evaluated in terms of obtained photocurrent, product selectivity, faradaic efficiency and stability, and the synergy between photo- and electro-induced mechanisms has been discussed. Thus, we believe that this study provides a meaningful reference for PEC technology in the solar-to-chemical energy conversion in academic research and industrial application.

2. Experimental section

2.1. Preparation of WO_3 photoanode

The synthesis procedure of monoclinic WO_3 was based on that reported in a previous study [66]. Typically, 0.6 g of WCl_6 (Sigma-Aldrich) was firstly dissolved in Ethanol (99.8% purity, Sigma-Aldrich) solution (120 mL) and transferred to a 200 mL of Teflon-lined stainless-steel autoclave for hydrothermal treatment at 180 °C for 12 h. Then, the light-blue WO_3 was carefully withdrawn and washed using Ethanol and deionized water 3 times. The collected powder was dried at 80 °C overnight. Finally, the bright yellow monoclinic WO_3 with high crystallinity and suitable oxygen defects (with a ratio of W^{5+}/W^{6+} of ~0.18/0.82 as determined in ref [40]) was obtained by post-calcination treatment at 450 °C for 1 h (5 °C min^{-1} of heating rate) in air. Samples were well-grinded before use. A catalyst ink was prepared by mixing the obtained WO_3 catalyst powder with a 5 wt% Nafion (Sigma-Aldrich) perfluorinated resin solution in aliphatic alcohols and water (to reach a WO_3:Nafion wt. ratio of 1:1) and 5 mL isopropanol (HPLC-isocratic grade, Carlo Erba Reagents). Then, the ink was sprayed with an aerograph on a carbon cloth (W1S1011, FuelCellStore) electrode-support with a thickness of 410 μm and an area of 5.3 cm^2. The alcohol/water solvent was evaporated at 80 °C, and the catalyst loading on the carbon cloth was controlled by weight measurement, reaching a value of 3.5 mg cm^{-2}. Details on the physicochemical characterizations of this WO_3 material can be found in our previous publication [40].

2.2. Membrane Electrode Assembly (MEA) and PEM cell setup

The synthesized carbon cloth-supported WO_3 was used as the photoanode, and a commercial carbon cloth-supported Pt (20% wt.)/C (Fuel Cell Store) with a loading of 0.2 mg·cm^{-2} was used as cathode. In the latter case, the carbon cloth behaves as gas diffusion layer (GDL) with a microporous layer (MPL) and a thickness of 365 μm. In the former case, the carbon cloth with a MPL and a thickness of 410 μm serves as a substrate which is a low-cost alternative to GDL materials. A Nafion™ 117 membrane was used as the proton-exchange membrane (PEM) with a thickness of 183 μm, which does not only serve as a solid electrolyte, but also as a physical separator for the obtained redox products. Prior to assembly, the membrane was pretreated by successive immersions in 3 different 150 mL-solutions, 3% wt·H_2O_2, 0.5 M H_2SO_4 and deionized water, in that order. The membrane electrode assembly (anodic photoelectrode/PEM/cathodic electrode) was prepared by hot-pressing under 1 metric ton at 120 °C for 3 min. In this MEA, the anode electrode was placed facing the membrane by the carbon cloth side that was not sprayed with the catalyst ink, while the commercial cathode electrode was placed facing the membrane by the catalyst-MPL side (Fig. 1).

The employed (photo)electrochemical cell was adapted from a 5 cm^2-commercial electrochemical cell (Dioxide Materials), by designing and constructing one of the two bipolar plates, i.e., the anode

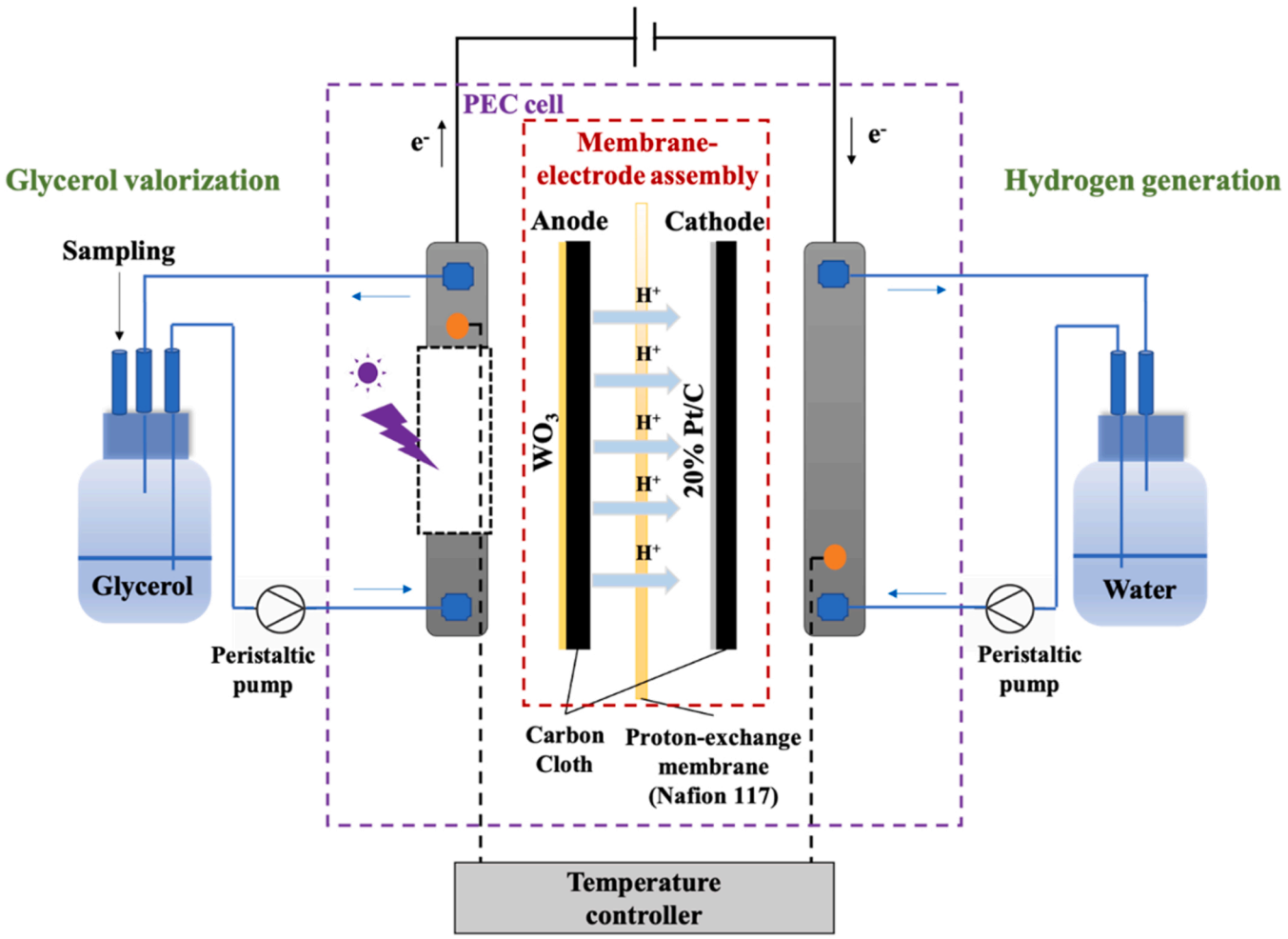

Fig. 1. Scheme of the Proton-exchange membrane (PEM) photoelectrocatalytic (PEC) cell set-up employed in this study.

side, to house a suitable quartz window for the PEC measurements. The PEC was also modified to introduce heating resistance rods (see Fig. S1 in Electronic Supplementary Information). The MEA was held between two Teflon gaskets to ensure the correct sealing of the Photoelectrolyser and was placed in a way that the catalyst-sprayed side of the photoanode faces the cell window (3.8 cm^2). As depicted in Fig. 1, a temperature control system was used, and 30 mL-solutions of 0.1 M glycerol and pure water (pH 5.5 both) were continuously fed (recycled) by means of a peristaltic pump (ISMATEC SA, Switzerland) through the anode and cathode sides of the cell from the respective reservoirs at a flow rate of approximately 3 mL min^{-1} each.

2.3. Electrochemical characterization

An Origalys OGBO5A electrochemical station (OrigaLys ElectroChem SAS, Rillieux-la-Pape, France) was used to measure the photoelectrochemical properties of the PEC PEM system, by feeding either 0.1 M glycerol or pure water to the anodic side of the cell, while feeding pure water to the cathodic side. Photocurrent, linear sweep voltammetry (LSV), cyclic voltammetry (CV), and open circuit potential (OCP) measurements were performed. The transient photocurrent tests were carried out at different applied cell potentials from 0.3 V to 1.5 V with 15 s of irradiation interval, using a LED UV lamp as the light source (41 mW cm^{-2}), with an incidence area of 1 cm^2. Prior to these measurements, the system was kept in dark conditions for 2 min to stabilize the current derived from the external bias. CV was recorded between 0 and 1.5 V (cell potentials) at a scan rate of 10 mV s^{-1} for 10 cycles under light irradiation. All the tests presented in this study were carried out in the same system, without changing the electrodes nor the membrane.

2.4. TC/PC/EC/PEC glycerol oxidation

PEC experiments were carried out under ultraviolet light using the same setup and LED UV lamp above mentioned. The PEC was measured under different applied cell voltages, between 0.3 and 1.2 V, and at different temperatures between 25 and 80 ºC. Purely PC, EC and TC experiments were also carried out at different cell temperatures in the absence of either external bias, light irradiation or both, respectively. Prior to all measurements, the cell and all lines of the experimental setup were systematically deeply cleaned. Then, the anolyte and catholyte solutions were initially flowing through the cell for 30 min under dark and open-circuit conditions, at room temperature, to achieve the adsorption-desorption equilibrium of glycerol on the surface of the WO_3 catalyst. Then, the PEC/PC/EC/TC measurements were initiated and, every hour, a sample (0.6 mL) was collected from the anode solution and immediately filtered by a Millipore 0.45 μm (hydrophilic PVDF) membrane using a plastic syringe. The reaction time was generally 6 h, except for the long-term experiment (27 h). The concentrations of glycerol and derived products were analyzed by a Shimadzu SPD-M20A ultrafast high-performance liquid chromatography (HPLC) equipped with a Transgenomic ICSep ICE-COREGEL-87H3 organic acid column. 5 mmol L^{-1} of H_2SO_4 with a flow rate of 0.7 mL min^{-1} served as the mobile phase and the column temperature was 30 °C. The products of

glycerol oxidation were determined by the ultraviolet detector at the wavelength of 210 nm. Glycerol was analyzed by the refractive index detector (RID). The concentration of total organic carbon (TOC) of the solutions before and after the PEC tests were measured using a Shimadzu TOC-VCPN analyzer equipped with an auto-sampler.

According to the liquid products detected, the photo- (or electro-) catalytic reactions (1−5) were assumed to take place on the WO_3 catalyst surface, by considering the transfer of either holes left in the valence band (h^+_{VB}) upon illumination (under PEC or PC operation conditions) or electrons (e^-, under EC conditions).

$$C_3H_8O_3 + 2h^+_{VB}(-2e^-) \rightarrow 2H^+ + C_3H_6O_3(\mathrm{GAD/DHA}) \quad (1)$$

$$C_3H_8O_3 + 2H_2O + 8h^+_{VB}(-8e^-) \rightarrow 8H^+ + C_3H_4O_5(\mathrm{tartronic\ acid}) \quad (2)$$

$$2C_3H_8O_3 + 3H_2O + 10h^+_{VB}(-10e^-) \rightarrow 10H^+ + 3C_2H_4O_3(\mathrm{glycolic\ acid}) \quad (3)$$

$$2C_3H_8O_3 + 6H_2O + 22h^+_{VB}(-22e^-) \rightarrow 22H^+ + 3C_2H_2O_4(\mathrm{oxalic\ acid}) \quad (4)$$

$$C_3H_8O_3 + 3H_2O + 8h^+_{VB}(-8e^-) \rightarrow 8H^+ + 3CH_2O_2(\mathrm{formic\ acid}) \quad (5)$$

The total amount ($N_{t,i}$, in mmol) of unreacted glycerol and of each produced chemical, i, at a given time (i.e., sampling time), t, was calculated from the concentration values quantified by HPLC, according to Eq. (6):

$$N_{t,i} = V_t \times C_{t,i} + V_s \times \sum_{t=0}^{t-1} C_{t,i} \quad (6)$$

where V_t (in L) and $C_{t,i}$ (in mM) are the solution volume and the concentration of the chemical i in the cell, respectively, at the time t, V_s is the sample volume (i.e., 6 $\times 10^{-4}$ L) and, thus, the term $[V_s \times \sum_{t=0}^{t-1} C_{t,i}]$ stands for the accumulated amount of product or unreacted glycerol collected in previous samplings.

The Glycerol conversion (in %) at a given time was calculated according to Eq. (7):

$$Glycerol\ \ conversion(\%) = \frac{V_0 x C_{0,glycerol} - N_{t,glycerol}}{V_0 x C_{0,glycerol}} \times 100 \quad (7)$$

Where V_0 (in L) and $C_{0,\mathrm{glycerol}}$ (in mM) stand for the initial electrolytic solution volume and glycerol concentration, respectively, and $N_{t,\mathrm{glycerol}}$ is the unreacted amount of glycerol at a given time, t.

The Yield (in %) and the Selectivity (in %) of every product were calculated at a given time, t, according to Eqs. (8) and (9), respectively:

$$Yield(\%) = \frac{N_{t,i}}{V_0 x C_{0,glycerol} x f_i} \times 100 \quad (8)$$

$$Selectivity(\%) = \frac{N_{t,i}}{(V_0 x C_{0,glycerol} - N_{t,glycerol}) x f_i} \times 100 \quad (9)$$

where f_i is the stoichiometric factor of the product i with respect to glycerol (i.e., according to reactions (1−5)).

Then, for EC and PEC comparison, the faradaic efficiency of each target product, FE (in %) was calculated through Eq. (10).

$$FE = \frac{N_i}{N_e} \times 100 \quad (10)$$

Where N_i and N_e (in mmol) stand, respectively, for the number of electrons/holes that would be transferred for production of the quantified amounts of product i under EC/PEC conditions, and those electrochemically transferred according to the measured electric charge, Q (in C), which can be calculated, at a given time, through Eqs. (11) and (12):

$$N_i = n_{e,i} \times N_{t,i} \quad (11)$$

$$N_e = \frac{Q}{F} \times 1000 = \frac{\int_0^t I\ dt}{F} \times 3600 \quad (12)$$

Where $n_{e,i}$ is the number of mol of electrons/holes theoretically transferred for the production of each mol of target product i (i.e., according to reactions (1−5)), F is the Faraday constant (96,485 C $mol_{e^-}^{-1}$) and I (in mA) is the current obtained at a given time, t (in h).

3. Results and discussion

3.1. Photoelectrochemical characterization

The homemade WO_3 photoanode was coated on a commercial carbon cloth and tested in the PEC proton-exchange membrane (PEM) cell shown in Figs. 1 and S1, where a commercial Pt/C electrode behaved as the cathode. Through the quartz window, the UV light with a radiation density of 41 mW cm^{-2} activates the photocatalyst to excite electrons to the conduction band (e^-_{CB}), leaving the same number of holes in the valence band (h^+_{VB}), which may participate in the glycerol valorization (reactions (1−5)) and/or water oxidation (reactions (13−14)). Meanwhile, the resultant protons and electrons are transferred to the cathode through the proton-exchange membrane and the external circuit, respectively, leading to the hydrogen evolution reaction (HER, reaction (15)). Hence, the external bias contributes to separating the photogenerated electrons from the holes, thus hindering their recombination and increasing the holes availability for oxidation reactions, while the PEM configuration is expected to improve the EC performance and allows the elution of a purified H_2 cathodic stream.

$$H_2O + 2h^+_{VB} \rightarrow 2H^+ + 1/2O_2 \quad (13)$$

$$2H_2O + 2h^+_{VB} \rightarrow 2H^+ + H_2O_2 \quad (14)$$

$$2H^+ + 2e^-_{CB} \rightarrow H_2 \quad (15)$$

Transient photocurrent response tests were performed at different applied cell potentials (0.3, 0.6, 0.9, 1.2 and 1.5 V) and temperatures (25, 40, 60 and 80 °C) to investigate the photoelectrochemical performance of the synthesized photoanode in 0.1 M glycerol (Fig. 2). The typically observed first sharp decrease of the current for the first seconds is mainly due to the decay of the capacitive current, after which rather stable photocurrents have been obtained in all cases. Both currents and photocurrents increase with the cell voltage at any reaction temperature. One can observe that this PEM PEC system is electrocatalytically active in a potential range (0.3–1.5 V) in which other WO_3-based photoanodes [17,39,40,66] were inactive in a 3-electrodes cell configuration under dark conditions. Indeed, the high contribution of the electrocatalytic activity likely diminished the effect of the increase of the photocurrent due to the light irradiation. It suggests that the PEM configuration implies an especially important upgrading from the electrocatalytic (rather than photocatalytic) point of view. It could be attributed to the compactness of the MEA configuration, which leads to presumably much lower ohmic losses between anode and cathode, as well as stronger interaction between the catalyst/support/electrolyte three-phase boundaries, than a 3-electrodes cell. Also, the use of carbon cloth as catalyst support and gas diffusion electrode herein increases the electrode roughness and enhances the diffusion of reactants and products, thus favouring their access to the catalyst active sites. For instance, at 60 °C, the obtained current (in the dark) was enhanced from 0.4 to 3.1 mA at cell voltages from 0.3 to 1.5 V, with photo-induced current increments from 0.1 to 0.5 mA, respectively, upon illumination, which denotes a slight increasing trend of the generated photocurrent with the applied voltage.

The rise of the temperature also favored the obtained currents, reaching a value at 1.5 V that was four times higher at 80 °C than that at 25 °C. However, this influence was much less pronounced on the photo-

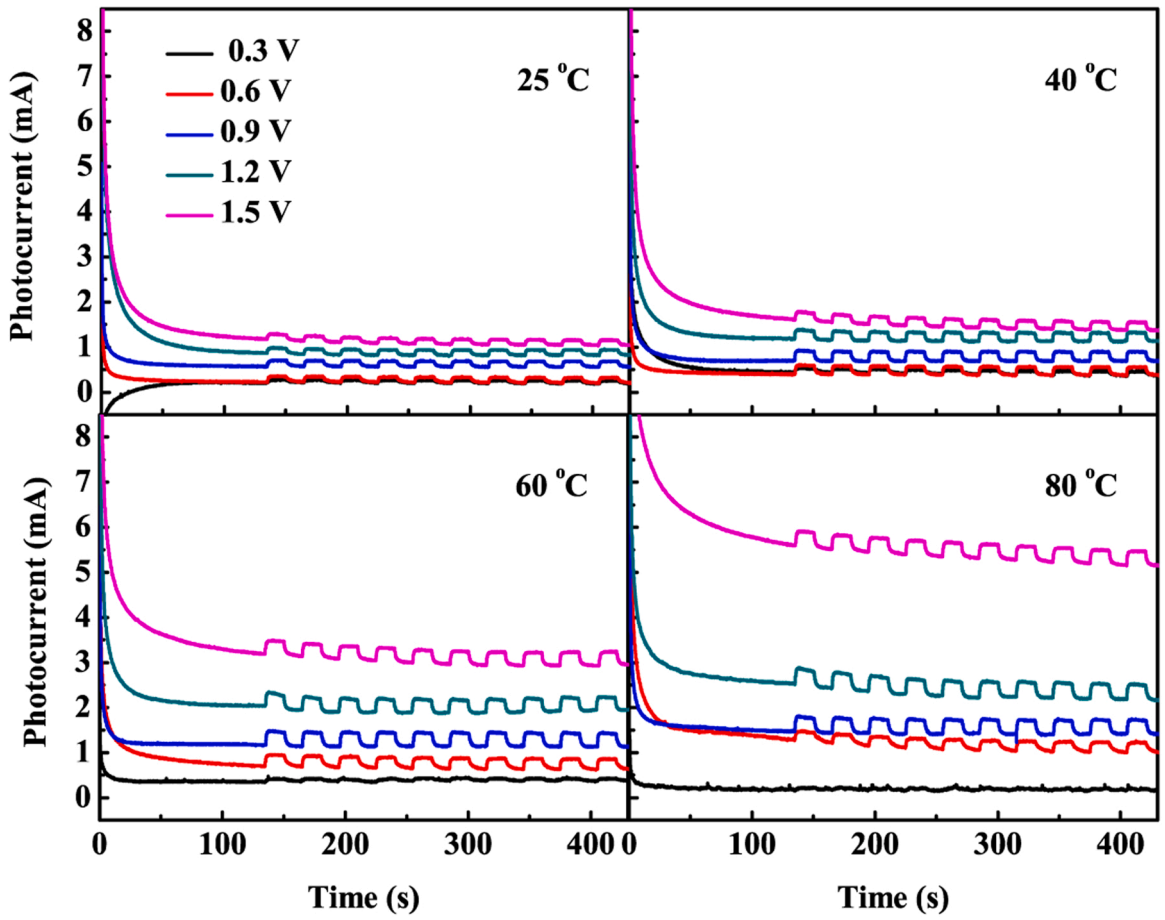

Fig. 2. Transient photocurrent response at different cell voltages (0.3–1.5 V) and temperatures (25–80 °C). Anode: WO_3/carbon cloth; cathode: Pt (20 wt%)/C/carbon cloth; Membrane: Nafion 117; anodic solution: 0.1 M glycerol (30 mL); cathodic solution: water (30 mL). Each pulse of current corresponds to an illumination of UV light pulse of 41 mW cm^{-2}.

generated currents, with similar current increases upon illumination above 40 °C, which can be attributed to a likely detrimental temperature effect on the charge carriers' separation [67,68]. On the other hand, if we compare these transient photocurrent tests in the presence of glycerol (Fig. 2) with those performed in pure water at the same temperatures and applied potentials (Fig. S2), we can observe that the obtained current intensities in the dark are all in the same range and are probably strongly related to the large capacitive current of the photoanode, as typically found on carbon-supported photoanodes [69], and maybe also to its EC activity for water electrooxidation in the experiments performed at 1.5 V. However, very interestingly, there is a significant increase in the photo-generated current upon irradiation in the presence of glycerol, which acts as a hole-scavenger and benefits the separation of photo-induced charges [70,71]. It should also be noted that the photocurrent densities obtained in this work are lower than those reported in other studies with conventional 3-electrodes PEC cells, for instance using $BiVO_4$-based photoanodes [25,38]. However, the performance of the WO_3 electrode used herein would be expected to improve after a further upgrading in terms of morphology, structure and composition.

Cyclic voltammetry (CV) tests have also been performed upon UV irradiation, and the 10th cycle obtained at each temperature is shown in Fig. 3, both in the presence and in the absence of glycerol. At low cell potential (0–0.3 V), apart from some cathodic hydrogen evolution on the WO_3 electrode, cathodic and anodic peaks were expected due to the intercalation/de-intercalation of H^+ in the WO_3 [72–74]. Then, during the forward scan in pure water (Fig. 3a), an increase in the anodic current can be observed at 0.5–0.6 V, likely due to the intercalation of oxygen into the vacancies of the photoanode oxide network [75,76], followed by the oxygen evolution curve at higher potentials. On the other hand, in the presence of glycerol (Fig. 3b), the anodic peaks obtained at low potentials were likely overlapped with the current increase derived from glycerol oxidation. Indeed, under cell voltages below c.a. 0.7 V, the obtained currents are higher in glycerol solution than in pure water (e.g., 2.4 mA with 0.1 M glycerol vs. 1.8 mA with pure water at 0.6 V and 80°C), which can be attributed to the low onset oxidation potential of glycerol oxidation (typically lower than 0.4 V vs. RHE on W-based electrodes [25,39,40]). Then, in the potential range of 0.7–1.5 V, the currents obtained in the presence of glycerol are lower, and a reasonable hypothesis is the partial poisoning of the catalyst surface by adsorbed reaction intermediates at this potential range. However, as the potential or temperature are further increased and these surface species are desorbed/oxidized, the currents obtained in glycerol solution reach again similar values than those obtained in pure water (e.g., 6.6 and 6.7 mA, respectively, at 1.5 V and 80°C), derived from the contribution from oxygen evolution reaction and the oxidation of fresh glycerol and its derived molecules.

Thus, from the transient photocurrent and CV measurements, it is clear the beneficial influence of both the cell voltage and temperature on the overall photo-electro-catalytic activity of the PEM Photoelectrolyser. It is worth noting that, under given PEC operation conditions, the expected hydrogen production rate in this PEM cell is directly related to the obtained current intensity, since both glycerol oxidation and water oxidation reactions at the anode imply the reduction of protons at the cathode. Thus, regardless of the products obtained in the anodic side of the cell, an increase in both parameters, i.e., potential and temperature, was found to be beneficial when dealing with the maximization of the

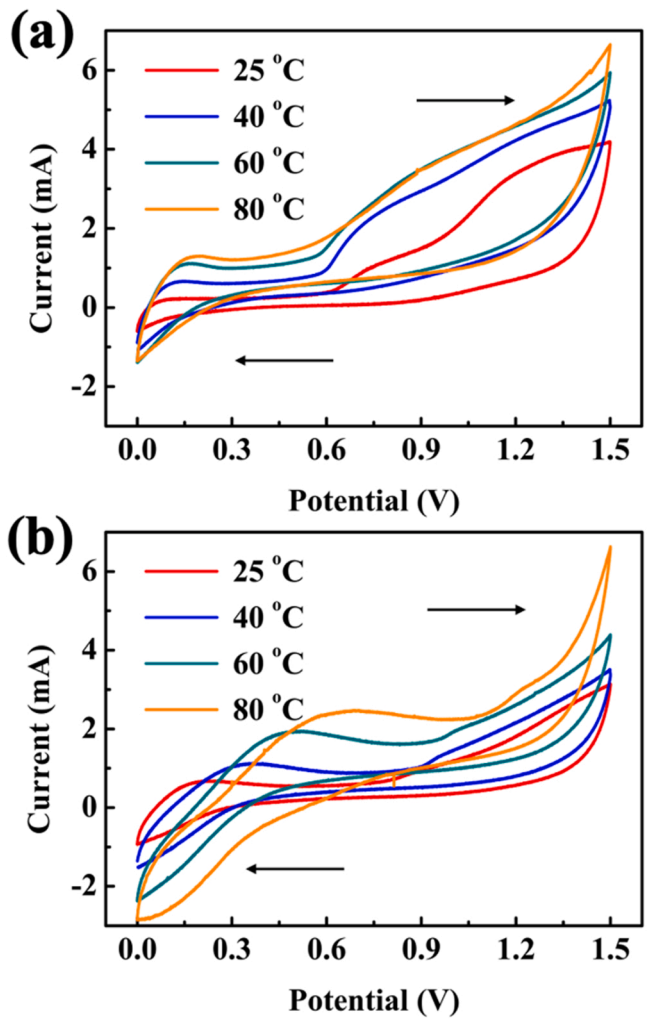

Fig. 3. Cyclic voltammetry (CV) performed in the Photoelectrolyser at different temperatures (25–80 ºC) under UV light irradiation (41 mW cm^{-2}) using (a) water or (b) 0.1 M glycerol as anodic solution, and water as cathodic solution. Scan rate: 10 mV s^{-1}. The 10th cycle is shown in each case. Anode: WO_3/carbon cloth; cathode: Pt (20 wt%)/C/carbon cloth; Membrane: Nafion 117.

obtained current intensity and, therefore, of the hydrogen production on the cathode side (reaction (15)). However, for the optimization of the bifunctional Photoelectrolyser, the anodic performance for biomass valorization (in terms of products selectivity) must be also evaluated.

3.2. Glycerol valorization by PEC

The operation conditions of the PEM PEC system have been optimized for the selective glycerol valorization to produce high-value-added products, by focusing on the obtained liquid products, and with special interest in GAD and DHA, claimed as the most valuable ones.

3.2.1. Effect of cell voltage

In all the tests, under light irradiation on the WO_3 photoanode, GAD and DHA were obtained as the main products, along with some formic acid (FA) and trace amounts of glycolic (GA), tartronic (TA), and oxalic (OA) acids. Other unknown product was also detected by HPLC in some cases and, given that the overall liquid products selectivity remained below 100% in all cases, significant amounts of CO_2 were also expected to be evolved, derived from glycerol mineralization. However, it should be noted that the use of a PEM membrane to separate anodic and cathodic compartments still ensures the elution of pure H_2 gas stream from the latter in any case. Fig. 4a-c and d-f show the dynamic results obtained at 60ºC under photocatalytic (PC) conditions (i.e., in the absence of any electric polarization) and under PEC conditions at 1.2 V, respectively, while Fig. S3 shows those obtained under intermediate cell voltages between 0.3 and 1.2 V. Note that all concentration profiles shown in the manuscript refer only to the anodic liquid products that have been properly identified. In all cases, one can observe that the concentration of the target liquid products in the cell linearly increased with time, leading to constant production rates (11.1 and 5.2 mmol m^{-2} h^{-1} for GAD and DHA, respectively) upon increasing glycerol conversion with an average consumption rate of 42.0 mmol m^{-2} h^{-1}. Thus, increasing yields and larger or, at least, stable selectivities were obtained with the reaction time. When comparing the obtained GAD production rate with those reported in the field of electrocatalytic glycerol oxidation, it is noteworthy that there are only two studies using flow-through electrochemical reactors where GAD was quantitatively generated, by means of Pt-based anodes. The GAD production rate obtained herein on the WO_3 photoanode in the near-neutral media is similar to that obtained at 60ºC using a Pt/C catalyst and a Nafion membrane (15.6 mmol m^{-2} h^{-1}) [51], and lower than that reported with a membrane-less configuration at room temperature using a Pt_9Bi_1/C catalyst (1950 mmol m^{-2} h^{-1}) [77]. However, in the latter case, strongly alkaline conditions were employed (0.5 M NaOH) and the glycerol feeding rate was also two orders of magnitude higher than in the present work (40 vs. 0.3 mmol min^{-1}).

Regarding the external bias influence, in our previous study using a similar WO_3 photoelectrode for the selective glycerol oxidation in a conventional PEC reactor, the light showed to be the trigger of the reaction while the external voltage seemed to promote the separation of photogenerated electrons and holes in the photocatalyst, thus raising the PEC activity and the GAD and DHA yields, in particular, highlighting the promising properties of this photoelectrode for the selective glycerol valorization [40]. A similar promoting effect of the external bias on the DHA and GAD yields was observed in the PEM Photoelectrolyser (Fig. 5). Under purely PC conditions, GAD and DHA were already selectively generated with a cell concentration after 6 h of 0.50 and 0.26 mmol L^{-1}, respectively. Their production was very similar upon 0.3 V but increased upon the application of higher cell voltages to reach 1.29 and 0.61 mmol L^{-1} for GAD and DHA after 6 h, respectively. Similar glycerol conversions were reached under all applied potentials after 6 h-test, i.e., 4.2–4.7%. Given the negligible current obtained at low potentials (i.e., 0.3 V, Fig. S4a) the conversion observed under such conditions is rather attributed to a bare thermo-catalytic decomposition of glycerol as will be shown below. However, what is most interesting is that GAD and DHA yields were increased by more than 2 times from 0.3 V to 1.2 V (Fig. S3e-h). Indeed, in the case of GAD, the yield showed to increase linearly in this potential range, at a rate of 0.82% V^{-1}. On the other hand, the GAD+DHA selectivity gradually increased with the applied potential from c.a. 15.2% (0.3 V) to 38.3% (1.2 V) (Fig. S3i-l). With respect to purely PC conditions (Fig. 4), the GAD and DHA selectivity only slightly increased, but the corresponding glycerol conversion more than doubled by PEC at 1.2 V after 6 h on stream. This explains the enhanced yield of the desired products at 1.2 V compared with the purely PC conditions. Besides, the influence of the potential was even greater on the obtained current, and therefore on the hydrogen production at the cathode (Figs. 5 and S4a).

Given the important competition of glycerol overoxidation reactions expected in the studied potential range, the enhanced $C_{3\,s}$ selectivity by PEC upon increasing potentials is of especial relevance. Apart from being the first photoelectrocatalytic study of glycerol oxidation in a PEM-type cell, the obtained selectivity results also stand out with respect to the published works on purely electrocatalytic systems. Table 1 collects a selection of results obtained on glycerol electrooxidation in all kinds of flow-through cells, like compact PEM electrolysers [51–56], other flow reactors employing polymer electrolyte membranes [57–59, 78] and recently explored membrane-less configurations [77–81]. Although the glycerol conversion values in literature (the reported ones)

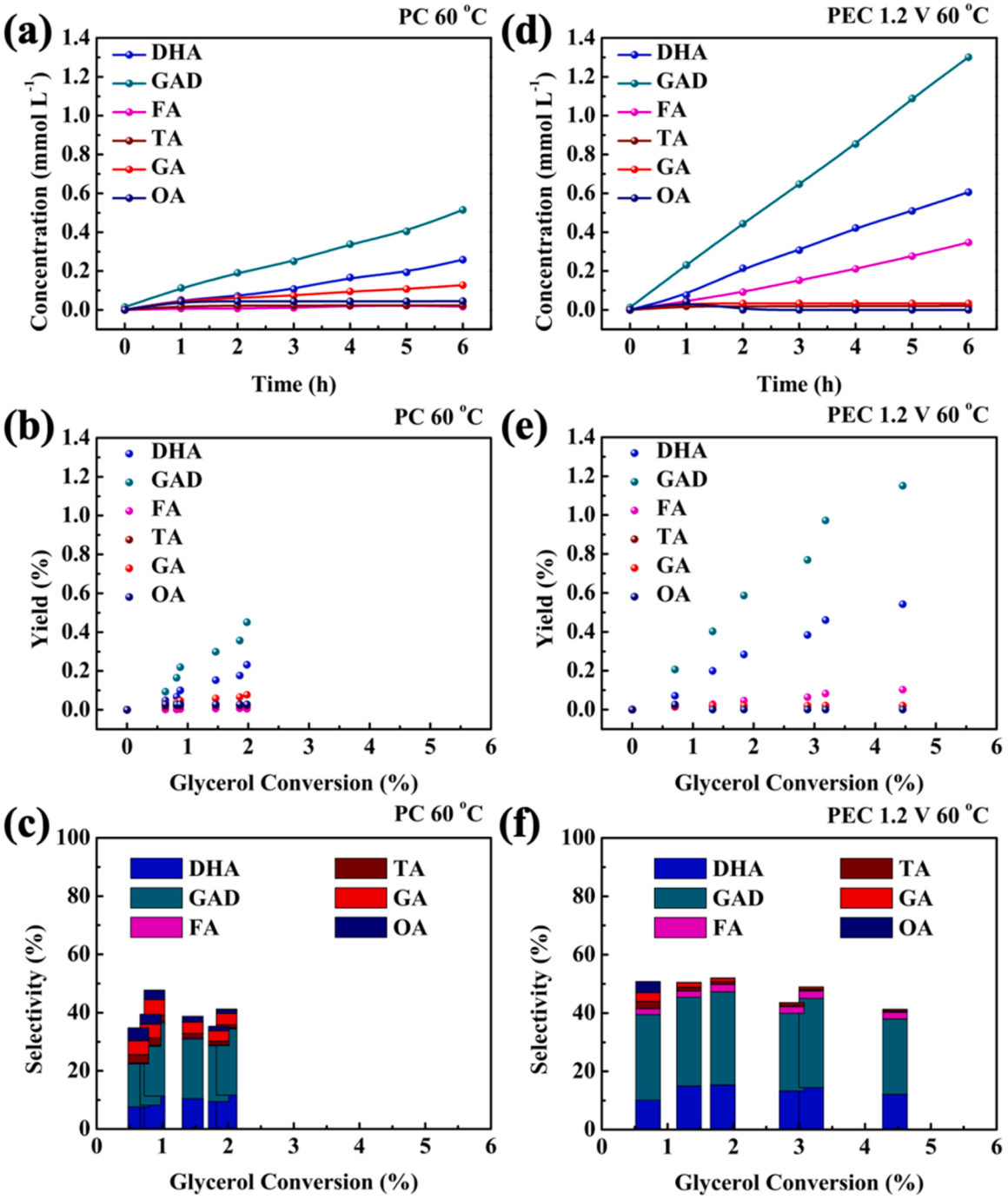

Fig. 4. (a,d) Time evolution of liquid products concentration in the anodic solution, and evolution of (b,e) yield and (c,f) selectivity of liquid products with glycerol conversion, during experiments performed under photocatalytic (PC) conditions and PEC at 1.2 V. Anode: WO_3/carbon cloth; cathode: Pt (20 wt%)/C/carbon cloth; Membrane: Nafion 117. Cell temperature: 60 °C. Initial glycerol concentration in anodic solution: 0.1 M. Initial volume of anodic solution: 30 mL. UV irradiation intensity (PEC): 41 mW cm^{-2}.

were in several cases higher than those obtained herein, one can stress that most of the anodes were tested in strongly alkaline electrolytes and proved to be completely unselective for GAD or DHA. The main products usually are GRA, TA or FA, with only two cases where bulk GAD production was reported using platinum-group metal (PGM) catalysts [51,77], as mentioned above. Moreover, it is also noteworthy that, in conventional EC systems, the increase of the applied potential, in the range studied herein, typically results in the generation of increasingly oxidized glycerol products (e.g., glyceric, hydroxypyruvic and tartronic acids), which is evident from the decrease of GAD selectivity with the cell voltage in the two aforementioned works [51,77]. This contrasts with the stable GAD and DHA selectivity obtained herein, likely due to the selective PEC behavior of the WO_3 material, and represents one of the main advantageous aspects of the proposed PEC technology compared to conventional EC. It must be also noted that, in terms of obtained current densities, those obtained in this work are c.a. 2 orders of magnitude lower than those reported with conventional EC glycerol electrolysers, as it is also typically found in the field of PEC water splitting [60–63]. This is likely influenced by the different nature of the materials employed as anodes/photoanodes and by the different light-

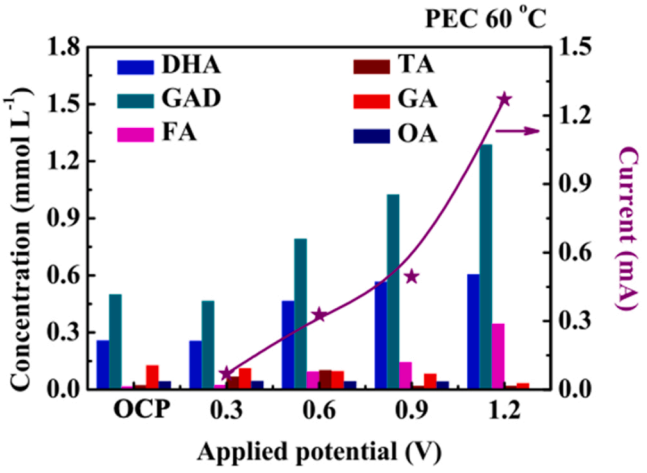

Fig. 5. Influence of the cell voltage on the liquid products concentration in the anodic solution and on the obtained current after 6 h. Anode: WO_3/carbon cloth; cathode: Pt (20 wt%)/C/carbon cloth; Membrane: Nafion 117. Cell temperature: 60 °C. Cell voltage: open circuit potential (PC) and 0.3–1.2 V (PEC). Initial glycerol concentration in anodic solution: 0.1 M. Initial volume of anodic solution: 30 mL. UV irradiation intensity (PEC): 41 mW cm^{-2}.

and electrolyte-exposed surface phenomenon taking place. However, the PEC approach offers the possibility of operating at lower voltages than conventional EC systems, with the consequent energy saving, while employing renewable energy sources. This, along with the outstanding C_3 selectivity found in this integrated system could make PEC an efficient and sustainable alternative technology for glycerol valorization after the proper photoelectrode engineering and operation conditions optimization.

3.2.2. Effect of cell temperature

Figs. 6 and S5 show the effect of cell temperature on the PEC performance, in the range from 25 to 80 ºC, at a fixed applied cell potential of 1.2 V, in order to provide the strongest possible capability to accelerate photo-induced charge separation without water oxidation occurrence. As opposed to the cell voltage, the temperature did not have a significant promoting effect on the PEC glycerol valorization. GAD and DHA production was only slightly enhanced by heating up to 60 °C and even decreased at 80 ºC. Although there are very few publications about the effect of reaction temperature on PC and PEC performances, in general terms, the temperature increase is expected to enhance the reaction kinetics and electrolyte conductivity, as reported for water splitting [82,83] and organic matter degradation [84,85]. For instance, Velázquez et al. [83] found a positive effect of the cell temperature in the PC production of H_2 from water and water/methanol solutions. However, the rise of the temperature may also hinder the charge carriers' separation, as recently reported, for instance, by Chen et al. [67]. These authors observed that the PC activity of TiO_2-based materials for the degradation of methylene blue decreased at temperatures higher than 70 ºC. Moreover, the temperature may also strongly influence the products' desorption and reactants' adsorption, which are typically considered the rate-limiting steps in PC systems at temperatures below 20 ºC and above 80 ºC, respectively [68,86]. For these reasons, the temperature range of 20–80 ºC seems to be optimum for the PEC

Table 1
Glycerol (GLY) oxidation selectivity reported with different flow-through electrochemical cells.

Cell configuration	Membrane / Separator	Anode	Anolyte	Operation conditions[a]	GLY conv. / %[a]	Main liquid products (Selectivity / %)[a,b]	Ref.
PEC PEM cell with MEA	Nafion 117	WO_3 / Carbon cloth	0.1 M GLY	60 ºC, 1.2 V, 6 h	4.5	**GAD** (26) + **DHA** (12) + FA (2) + GA + TA	This work
PEM cell with MEA	Nafion 115	Pt (20 wt%) / C	0.1 M GLY	60 ºC, 1 V, 5 h	9	GRA (80) + **GAD** (8)	[51]
	Nafion 212	Pt (20 wt%) / $RuIrO_x$	8.5 M GLY	70 ºC, 5 mA cm^{-2}, 0.5 h	Liquid products not analyzed		[52]
	Proton-exchange	CoNiCuMnMo / Carbon cloth	0.1 M GLY + 1 M KOH	RT, 10 mA cm^{-2}, 12 h	-	FA (FE = 93.5%)[c]	[53]
	KOH-doped PBI	PtRu / C (20 wt% metal)	1 M GLY + 4 M KOH	60 ºC, 20 mA cm^{-2}	-	TA (61) + GRA (31) + GA + LA	[54]
			2 M GLY + 4 M KOH	75 ºC, 80 mA cm^{-2}	-	TA (45) + GRA (36) + OA + FA + GA	[55]
	Tokuyama A006	Pd-(NiZn) / C / Ni mesh	1.1 M GLY + 2 M KOH	RT, 19 mA cm^{-2}, 15 h	-	TA (36) + GRA (35) + GA + OA + FA	[56]
3-electrode membrane-separated cell	Fumasep FAA-3-PK-130	NiO_x / O-MWCNT / Carbon paper	0.1 M GLY + 1 M KOH	1.5 V vs. RHE, 6 h	80	FA (55) + OA + GA + GRA + AA	[57]
		Ni_xB / Carbon paper	0.5 M GLY + 2 M KOH	1.54 V vs. RHE, 4 h	10	FA (55) + TA (17) + GA (11) + GRA + OA	[58]
		$LaFe_{0.31}Co_{0.69}O_3$ / Carbon paper	1 M GLY + 1 M KOH	1.59 V vs. RHE, 24 h	15	FA (17) + GA (6) + GRA + LA + OA + AA	[59]
	Fumasep FAA-3-PK-75	Ni_9Au_1 / C	2 M GLY + 2 M KOH	20 ºC, 1.5 V	-	FA (-)[d] + LA (-)[d]	[78]
Compact membrane-less cell	Filter paper	Pt_9Bi_1 / C / Carbon cloth	2 M GLY + 0.5 M NaOH	RT, 0.55 V, 4 h	6	**GAD** (80) + GRA (10) + HPA + TA	[77]
		Ni_8Pd_2 / C	0.1 M GLY + 1 M KOH	50 ºC, 1.3 V, 6 h	28	GRA (47) + FA (39) + GA + TA + OA + LA	[79]
		Ni_9Bi_1	0.1 M GLY + 1 M KOH	50 ºC, 1.3 V, 6 h	25	GRA (41) + FA (38) + TA + OA + GA + LA	[80]
		$Ni_{95}Bi_5$ / C	0.1 M GLY + 1 M KOH	75 ºC, 1.35 V, 3 h	< 10	FA (51) + GRA (31) + GA + TA + LA	[81]
		Ni_8Pd_2 / C	0.1 M GLY + 1 M KOH	20 ºC, 1.55 V, 6 h	73	FA (100)	[78]

[a]Data drawn or estimated from the information reported in the articles (RT: Room temperature; polarization in terms of cell voltage unless otherwise stated).
[b]Selectivity values for the main products obtained (minor when not specified). GAD: Glyceraldehyde; DHA: Dihydroxyacetone; FA: Formate; GA: Glycolate; TA: Tartronate; GRA: Glycerate; LA: Lactate; OA: Oxalate; AA: Acetate; HPA: Hydroxypyruvate.
[c]Faradaic efficiency (FE) values (selectivity not reported).
[d]In this case, the anodic glycerol oxidation is coupled with cathodic CO_2 reduction (mainly to CO). No quantitative data on glycerol conversion or anodic products selectivity.

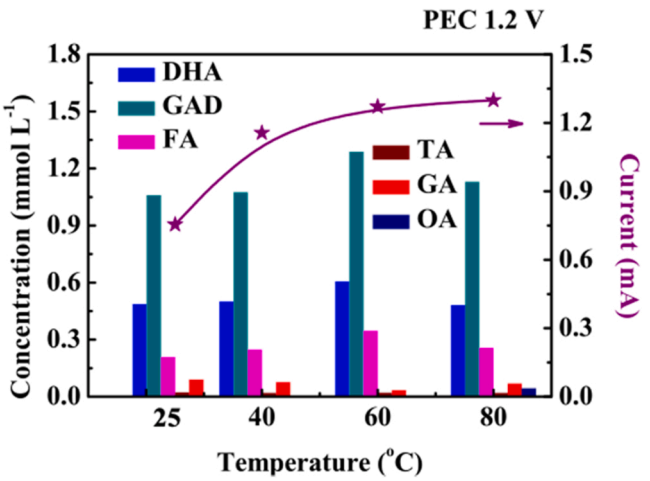

Fig. 6. Influence of the Photoelectrolyser temperature on the liquid products concentration in the anodic solution and on the obtained current after 6 h. Anode: WO_3/carbon cloth; cathode: Pt (20 wt%)/C/carbon cloth; Membrane: Nafion 117. Cell temperature: 25, 40, 60 and 80 °C. Cell voltage: 1.2 V. Initial glycerol concentration in anodic solution: 0.1 M. Initial volume of anodic solution: 30 mL. UV irradiation intensity: 41 mW cm^{-2}.

oxidation of organic matter. In the present work, the glycerol conversion values reached after 6 h-test slightly increased from 2.8% to 4.9% in this temperature range, with stable low GAD and DHA yields of 0.9–1.2% and 0.4–0.5%, respectively (Fig. S5e-h).

Regarding the selectivity obtained for the identified liquid products (Fig. S5i-l), the overall value after 6-hours test slightly decreased from 55% to 42% by heating from 25 to 60 ºC. In particular, fairly stable selectivity values of 26–34% and 12–16% were obtained for GAD and DHA, respectively. These values therefore denote a significant over-oxidation of glycerol and/or its derived products (> 50%) to CO_2 or other organic compounds, especially at 80 ºC, in which case the C_3 product selectivity clearly shows a decreasing trend with time and with the GLY conversion (Fig. S5l). Indeed, the amount of the aforementioned *unknown* liquid product detected by HPLC increased with the temperature (see Fig. S6). Likewise, the obtained current after 6 h seemed to find an optimum at 60 °C (Figs. 6 and S4b). As previously mentioned, this current can be directly related to the production of hydrogen at the cathode. Thus, in view of these experiments, we can conclude that the maximum operating temperature to enhance both the hydrogen generation (at the cathode) and the selective glycerol valorization (at the anode) by PEC is 60 ºC. Under these conditions, the application of an optimum cell voltage of 1.2 V allows to obtain stable GAD and DHA production rates at the anode side of 11.1 and 5.2 mmol m^{-2} h^{-1}, respectively, and a simultaneous H_2 production rate at the cathode side of 44.0 mmol m^{-2} h^{-1}, as estimated from a steady-state current intensity of c.a. 1.25 mA.

3.2.3. Stability evaluation

In order to evaluate the stability of the system, another PEC measurement was performed under relatively harsh conditions (1.2 V, 80 °C) for three successive days, with 3 successive operation periods of 9 h (27 h in total) (Fig. S7). After each pulse, the cell was cooled down to room temperature and the flow kept running. Results after 6 h are similar to those reported in Fig. 6 and, interestingly, the targeted value-added products, GAD and DHA, were still the main obtained products after 27 h, reaching yields of 3.6% and 1.5%, respectively, with a still low formic acid yield of 0.3% and an increase in the glycerol conversion up to ~ 40%, i.e., around 8 times higher than that reached in the short-term experiment (6 h), with an average consumption rate of 79.6 mmol m^{-2} h^{-1}. According to the continuous increase in glycerol conversion and the stable current intensity observed during this test (with a decrease of c.a. 0.1 mA in the last 24 h, Fig. S7e), the proposed PEM Photoelectrolyser using a WO_3 photoanode showed not only the capability for simultaneous hydrogen generation and glycerol valorization, but also a good stability in long-term operation. However, it should be noted that, under the studied operation conditions, GAD and DHA production rates slowed down for the last operation hours, with a presumably increase of CO_2 formation. Consequently, the joint selectivity of the targeted C_3 compounds continuously decreased for the 27 h-test, down to 13.4%. In view to the practical application of the PEC PEM cell for the selective glycerol valorization, higher solution volumes should be treated, thus operating under low-conversion conditions and, preferably, the targeted products should be continuously separated from the anode effluent and collected, in order to avoid their recycling and overoxidation. On the other hand, the repeatability of the PEC measurements has also been verified by replicating those performed under reference PEC conditions (an applied bias of 1.2 V and a cell temperature of 60ºC and 80ºC), as it can be observed in Fig. S8.

3.3. Technology comparison with EC, TC and PC

The PEC performance of the PEM cell for glycerol valorization has also been evaluated in a broader context by comparing the above-discussed results with those obtained at different temperatures under purely electrocatalytic (EC), photocatalytic (PC) and thermocatalytic (TC) conditions, i.e., by removing the light irradiation, the external bias, and both stimuli, respectively. An overview of the results obtained with the different technologies can be found in Fig. S9. Among them, the only technology capable to produce value-added organics and pure hydrogen gas separately, apart from PEC, is the electrocatalysis. In this way, glycerol electro-oxidation (reactions (1−5)) takes place on the WO_3 catalyst surface releasing protons and electrons that are transferred through the proton-exchange membrane and the external circuit, respectively, to the Pt cathode, where H_2 evolves. Figs. 7 and S9i-l show the liquid products distribution obtained by EC glycerol oxidation at different temperatures between 25 and 80 ºC under an applied cell voltage of 1.2 V. The temperature increase is expected to enhance the reaction kinetics, the mass transport and the membrane electrical conductivity. Indeed, the PEM cell configuration has been widely employed for hydrogen production from alcohols electro-reforming at temperatures closed to 80 ºC [48–50,52,54]. However, in the present case, although a significant EC activity for GAD production (0.382 mmol L^{-1})

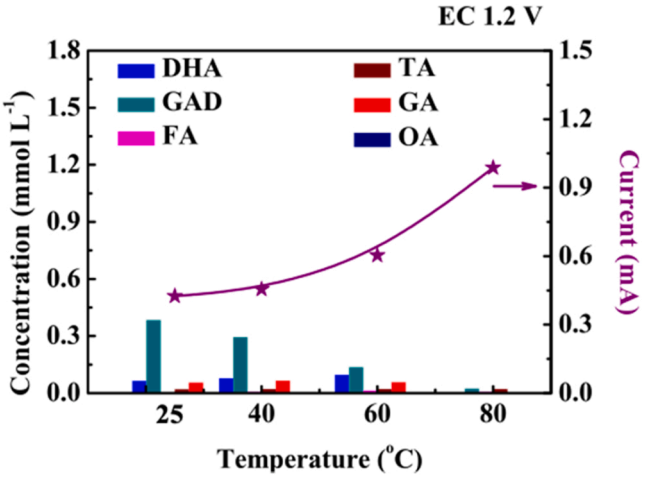

Fig. 7. Influence of the cell temperature on the liquid products concentration in the anodic solution and on the obtained current after 6 h under electrocatalytic (EC) conditions (without any illumination). Anode: WO_3/carbon cloth; cathode: Pt (20 wt%)/C/carbon cloth; Membrane: Nafion 117. Cell temperature: 25, 40, 60 and 80 °C. Cell voltage: 1.2 V. Initial glycerol concentration in anodic solution: 0.1 M. Initial volume of anodic solution: 30 mL.

was observed at room temperature, it was still much lower than that obtained by PEC of (1.059 mmol L^{-1}) and the heating showed a clear detrimental effect on the selective glycerol valorization, which became negligible at 80 ºC. Instead, the obtained currents increased with the temperature, as expected from the previous results on transient photocurrent measurements in dark conditions (Fig. 2). This enhanced EC activity can be mainly attributed to glycerol overoxidation reactions to gaseous CO_2 or other compounds which, in turn, are expected to be favored by hydroxyl or oxygen radicals generated from water [87,88].

The EC behavior is therefore different from that observed in PEC measurements, in which both the GAD/DHA production rates and the obtained currents were slightly enhanced with temperature up to 60 ºC (Fig. 6). Hence, if this dual compartment cell is used for pure EC reactions at 1.2 V, a high temperature is favorable for hydrogen production, while a low temperature is beneficial for selective glycerol valorization. Besides, a suitable external voltage is also necessary for the hydrogen generation by EC. For instance, at a low cell voltage of 0.3 V, the obtained current was negligible, even at 60 ºC (Fig. S10), and the observed glycerol oxidation products were likely derived from a purely thermocatalytic (TC) process, as can be observed in Fig. S9. Glycerol can be fully converted into DHA, glyceric acid or other organic compounds by TC at temperatures between 25 and 160 ºC by using 1–10 bar oxygen, as reviewed by Dodekatos et al. [89]. In this work, the measurements carried out in the absence of any light irradiation or external bias showed a negligible TC activity of the WO_3 catalyst at room temperature, but significant GAD production rates were observed upon increasing the temperature (Fig. S9a-d), even overpassing those obtained by electrocatalysis, which can be attributed to the promoting effect of EC operation on organic molecules mineralization and thus CO_2 generation, as will be discussed below. On the other hand, it is important to note that under either PEC or EC conditions, not only fresh glycerol but any other organic product derived from concurrent EC/PEC/TC/PC conversion processes is prone to be further oxidized.

Regarding pure PC reactions (Fig. S9e-h), the WO_3 photoanode showed an important production of GAD, with an optimum temperature of 40 ºC in this case. As discussed in Section 3.2.2, the sensitivity to temperature in the range of 25–80 ºC mostly stems from the influence on the recombination efficiency of photogenerated electrons and holes in WO_3 [67,68]. This was also evidenced in the PEC measurements performed at different temperatures (Fig. 6) although, in this operation mode, the optimum value was 60 ºC. Another sign of the temperature effect on the PC activity was noticed by analyzing the time response of the open circuit potential (OCP) upon illumination (Fig. S11). At 25 ºC, the decay in the OCP for the first seconds under light irradiation was higher than that observed at 80 ºC, which could be linked to a higher photoactivity in the former case due to a higher accumulation of photogenerated electrons [69,90]. This pioneering analysis of the glycerol oxidation results obtained in all operation modes, i.e., PEC, PC and EC, demonstrates that PEC performance for glycerol valorization, in terms of target C_3-product yield, is not only better than that obtained by PC, due to the promotional effect of the external bias on the charge carriers separation, but also greater than the sum of the individual yields obtained by PC and EC, at a given cell temperature. The superior PEC performance was especially evident at high temperatures. In fact, at 80 ºC, the production rates of GAD, DHA and all other identified liquid products were negligible (with glycerol conversion values of 2–5%) in all configurations except in PEC.

The synergistic effect between photo- and electro-catalysis was also found in terms of obtained current intensity, and thus hydrogen generation. For instance, one can observe that the steady-state current intensities obtained by PEC at 1.2 V at different temperatures (Fig. 6) were higher than those obtained by EC (Fig. 7) in all cases, with enhancements from 32% (at 80ºC) to 154% (at 40ºC). This demonstrates that the application of an external potential facilitates the separation of the charge carriers and thus increases the availability of the photogenerated holes for the glycerol oxidation reactions. At the same time, the light irradiation and the consequent generation of those charge carriers can enhance the overall number of electrons transferred between the photoanode and the cathode for their consumption in HER. In other words, PEC technology proves to be the most promising among the explored technologies for the synthesis of both hydrogen and value-added C_3 compounds.

3.3.1. Electron transfer efficiency assessment

In order to get more insights into the reactions preferably taking place on the WO_3 photoanode, the faradaic efficiency (FE) obtained under the different PEC and EC operation conditions has also been evaluated, along with the total organic carbon (TOC) measurements. Fig. 8a shows the electric charges transferred in the EC and PEC measurements performed for 6 h-each at different temperatures, as calculated from the intensity vs. time curves. The accumulated charges transferred in the PEC reactions were 4.53, 6.93, 7.62 and 7.79 mA·h at 25, 40, 60 and 80 °C, respectively. These values are 1.77, 2.54, 2.10 and 1.32 times higher than those obtained in pure EC processes at the corresponding temperatures (PEC/EC ratios in Fig. 8a). The charge

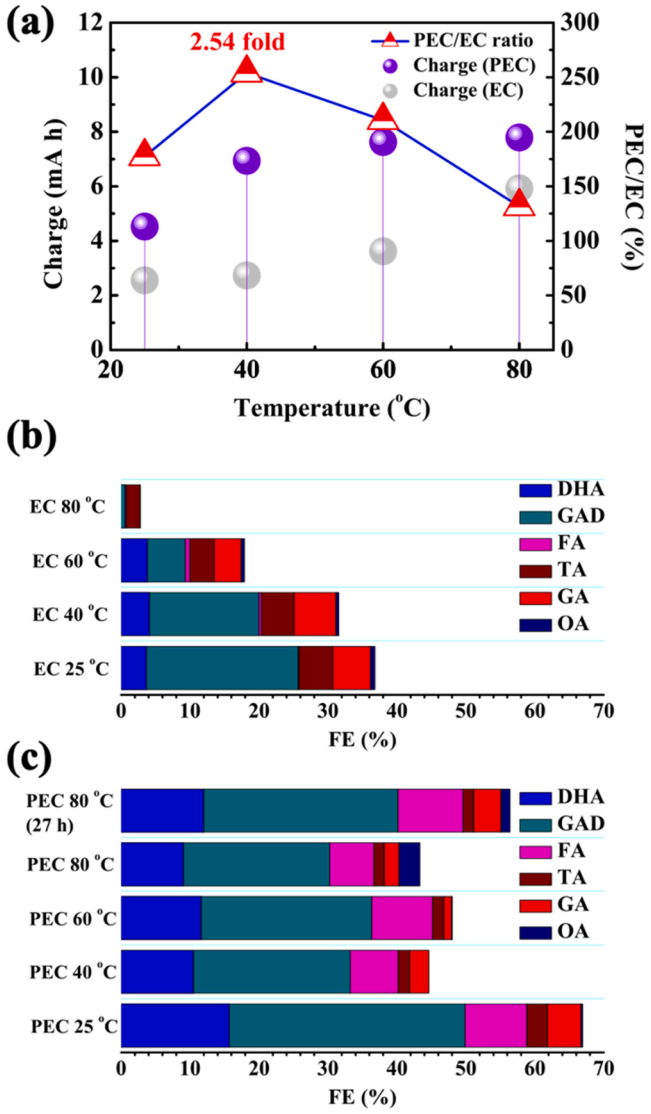

Fig. 8. (a) Comparison of the charge transferred during electrocatalytic (EC) and photoelectrocatalytic (PEC) processes at 1.2 V and different temperatures (25–80 ºC) as well as the enhancement PEC/EC ratio; Faraday efficiencies (FE) of liquid products in EC (b) and PEC (c) experiments. These data are associated with those shown in Figs. 6 and 7.

enhancement observed by increasing the temperature, and also by operating in the Photoelectrolyser configuration with respect to EC, can be linked to an increase in the consequent hydrogen production as above discussed. The improvements in the production rates of GAD and DHA by PEC vs. EC observed in the previous section were even greater than the respective increases in the transferred charges, which denotes that the faradaic efficiency (FE) values of the selective glycerol valorization reactions were higher by PEC than by EC, as can be observed in Fig. 8b and c.

The influence of the temperature on the faradaic efficiency was different depending on the operation mode, i.e., EC or PEC. The FE values obtained for the targeted C_3 products by pure electrocatalysis strongly decreased with the temperature, from 25.7% at room temperature to less than 1% at 80 ºC (Fig. 8b). This denotes that, in dark conditions, the increase in the electric charge transferred from the WO_3 catalyst with the temperature (Fig. 8a) is mostly attributed to the enhancement of glycerol overoxidation reactions, CO_2 probably being the main obtained product, especially at high temperature. However, in the tests performed under both light irradiation and external bias (Fig. 8c), the FE values obtained for GAD+DHA were higher and much more stable with the temperature, decreasing from 49.9% (25 ºC), to 30.3% (80 ºC). At this high temperature, the C_3 FE even increased to 40.1% when the measurement was extended from 6 to 27 h, indicating the good stability of C_3 FE. To understand this FE enhancement with time, one must take into account that the long-term decrease in the current density is more pronounced than the corresponding decrease in the C_3 production. The higher C_3 production by PEC is also evidenced by the higher stability of the TOC value obtained under these conditions. Fig. S12a and b show the variation of the TOC with the temperature under EC and PEC conditions, respectively. In the former case, a decreasing trend was obtained between 25 and 60ºC, with an average value of 3589 ± 82 mg L^{-1}, while the TOC was more stable in this temperature range under PEC conditions, with an average value of 3603 $\pm$ 33 mg L^{-1}. In the latter conditions, a significant TOC decrease was only observed at 80ºC. Thus, the results obtained in this operation mode seem to indicate that the increased number of electrons transferred under PEC conditions by increasing the temperature from 25 to 60 ºC is mainly derived from the selective glycerol oxidation reactions. One can conclude that, from the energy efficiency point of view, the Photoelectrolyser is also more favorable for the simultaneous hydrogen generation and glycerol valorization than the conventional EC configuration. These results open new doors in the application of the PEC approach to the electrolysis of organic molecules by easily adapting commercially available PEM cells, although further efforts should be made to maximize their photo- and photo-electrocatalytic features, for instance, by optimizing the light source, the light-exposed photoelectrode surface and, very specially, by tailoring more efficient photoelectrodes through the tuning of their nanostructure and/or composition.

4. Conclusions

A photoelectrocatalytic (PEC) cell with a proton-exchange membrane (PEM) configuration has been developed, for the first time, for the simultaneous glycerol valorization and green H_2 generation under soft pH conditions. For this purpose, a WO_3 catalyst which is selective for glyceraldehyde (GAD) and dihydroxyacetone (DHA) production has been employed as photoanode. The electrocatalytic (EC), photocatalytic (PC) and thermocatalytic (TC) effects have been assessed and the following conclusions can be drawn from this study:

- An increase of the temperature and, specially, of the voltage enhances the current generated by the photoelectrolyser, and thus the hydrogen production rate at the cathode. The cell voltage has also a positive effect up to 1.2 V on the selective glycerol oxidation to C_3 compounds at the anode, in contrast to conventional EC systems, due to the enhanced photogenerated charge carriers' separation.
- Under optimum PEC operation conditions, 60 ºC and 1.2 V, stable GAD and DHA production rates of 11.1 and 5.2 mmol m^{-2} h^{-1} are obtained, respectively, along with the simultaneous production of 44.0 mmol H_2 m^{-2} h^{-1}. Under such conditions, the selectivity of GAD+DHA reaches 38% after 6 h operation, corresponding with 4.5% glycerol conversion.
- In this PEM configuration, the WO_3 photoanode shows a much higher EC activity in dark conditions than conventional PEC systems operating in batch configuration. The increase of either the temperature (up to 80 ºC) or the cell voltage (up to 1.2 V) enhances the EC hydrogen production at the cathode and favours the deep oxidation of glycerol and/or its derived molecules, likely to CO_2, vs. glycerol partial oxidation at the anode.
- Under PC conditions, the catalyst shows a high selectivity for GAD production with an optimum operation temperature of 40 ºC. While the direct electron transfer from the anode under EC conditions favours the glycerol mineralization, the holes photogenerated by PC seem to be rather involved in the selective glycerol oxidation reactions to produce the targeted C_3 s.
- A strong synergistic effect is observed between electro- and photocatalytic effects. Thus, PEC proves to be the most promising among the explored technologies studied for the synthesis of both hydrogen and GAD/DHA in a PEM cell, as well as from the energy efficiency point of view.

CRediT authorship contribution statement

Jie Yu: Investigation, Conceptualization, Writing – original draft, Writing – review & editing, Visualization. **Jesús González-Cobos:** Formal analysis, Writing – review & editing. **Frederic Dappozze**: Resources, Formal analysis. **Nicolas Grimaldos-Osorio**: Resources, Formal analysis. **Philippe Vernoux**: Visualization, Formal analysis, Wriing – review & editing. **Angel Caravaca**: Visualization, Project administration, Supervision, Wriing – review & editing. **Chantal Guillard**: Funding acquisition, Project administration, Supervision.

Declaration of Competing Interest

The authors declare the following financial interests/personal relationships which may be considered as potential competing interests: Jie Yu reports financial support was provided by China Scholarship Council.

Data availability

Data will be made available on request.

Acknowledgments

This work was financially supported by the China Scholarship Council (Grant No. 201906740016). The authors would like to thank Frederic Bourgain (fabrication of Photoelectrolyser) of IRCELYON.

Declaration of Competing Interest

The authors reported no declarations of interest.

Appendix A. Supporting information

Supplementary data associated with this article can be found in the online version at doi:10.1016/j.apcatb.2023.122465.

References

[1] A. Dias da Silva Ruy, A. Luíza Freitas Ferreira, A. Ésio Bresciani, R. Maria de Brito Alves, L. Antônio Magalhães Pontes, Market Prospecting and Assessment of the Economic Potential of Glycerol from Biodiesel, in: Biotechnological Applications of Biomass, IntechOpen, 2021. ⟨https://doi.org/10.5772/intechopen.93965⟩.

[2] M.R. Karimi Estahbanati, M. Feilizadeh, F. Attar, M.C. Iliuta, Current developments and future trends in photocatalytic glycerol valorization: photocatalyst development, Ind. Eng. Chem. Res 59 (2020) 22330–22352, https://doi.org/10.1021/acs.iecr.0c04765.

[3] A. Mendoza, R. Romero, G.P. Gutiérrez-Cedillo, G. López-Tellez, O. Lorenzo-González, R.M. Gómez-Espinosa, R. Natividad, Selective production of dihydroxyacetone and glyceraldehyde by photo-assisted oxidation of glycerol, Catal. Today 358 (2020) 149–154, https://doi.org/10.1016/j.cattod.2019.09.035.

[4] M.S.E. Houache, K. Hughes, E.A. Baranova, Study on catalyst selection for electrochemical valorization of glycerol, Sustain Energy Fuels 3 (2019) 1892–1915, https://doi.org/10.1039/C9SE00108E.

[5] M.R.A. Arcanjo, I.J. da Silva Jr, C.L. Cavalcante Jr, J. Iglesias, G. Morales, M. Paniagua, J.A. Melero, R.S. Vieira, Glycerol valorization: Conversion to lactic acid by heterogeneous catalysis and separation by ion exchange chromatography, Biofuels, Bioprod. Bioref. 14 (2020) 357–370, https://doi.org/10.1002/bbb.2055.

[6] M. Simões, S. Baranton, C. Coutanceau, Electrochemical valorisation of glycerol, ChemSusChem 5 (2012) 2106–2124, https://doi.org/10.1002/cssc.201200335.

[7] T. Montini, V. Gombac, L. Sordelli, J.J. Delgado, X. Chen, G. Adami, P. Fornasiero, Nanostructured Cu/TiO_2 photocatalysts for H_2 production from ethanol and glycerol aqueous solutions, ChemCatChem 3 (2011) 574–577, https://doi.org/10.1002/cctc.201000289.

[8] Z.G. Schichtl, S.K. Conlin, H. Mehrabi, A.C. Nielander, R.H. Coridan, Characterizing Sustained Solar-to-Hydrogen Electrocatalysis at Low Cell Potentials Enabled by Crude Glycerol Oxidation, ACS Appl. Energy Mater. 5 (2022) 3863–3875, https://doi.org/10.1021/acsaem.2c00377.

[9] J. Gong, C. Li, M.R. Wasielewski, Advances in solar energy conversion, Chem. Soc. Rev. 48 (2019) 1862–1864, https://doi.org/10.1039/C9CS90020A.

[10] Y. Li, J. Li, W. Yang, X. Wang, Implementation of ferroelectric materials in photocatalytic and photoelectrochemical water splitting, Nanoscale Horiz. 5 (2020) 1174–1187, https://doi.org/10.1039/D0NH00219D.

[11] X. Lu, S. Xie, H. Yang, Y. Tong, H. Ji, Photoelectrochemical hydrogen production from biomass derivatives and water, Chem. Soc. Rev. 43 (2014) 7581–7593, https://doi.org/10.1039/C3CS60392J.

[12] A. Caravaca, W. Jones, C. Hardacre, M. Bowker, H_2 production by the photocatalytic reforming of cellulose and raw biomass using Ni, Pd, Pt and Au on titania, Proc. R. Soc. A: Math. Phys. Eng. Sci. 472, 2016: 0054. ⟨https://doi.org/10.1098/rspa.2016.0054⟩.

[13] A.K. Seferlis, S.G. Neophytides, Photoelectrocatalytic electricity and/or H_2 production from alcohols: the effect of TiO_2 film Thickness, J. Electrochem Soc. 158 (2010) H183, https://doi.org/10.1149/1.3522808.

[14] W. Sheng, Y. Song, M. Dou, J. Ji, F. Wang, Constructing 1D hierarchical heterostructures of MoS_2/In_2S_3 nanosheets on CdS nanorod arrays for enhanced photoelectrocatalytic H_2 evolution, Appl. Surf. Sci. 436 (2018) 613–623, https://doi.org/10.1016/j.apsusc.2017.11.281.

[15] N. Lakshmana Reddy, K.K. Cheralathan, V. Durga Kumari, B. Neppolian, S. Muthukonda Venkatakrishnan, Photocatalytic reforming of biomass derived crude glycerol in water: a sustainable approach for improved hydrogen generation using Ni $(OH)_2$ decorated TiO_2 nanotubes under solar light irradiation, ACS Sustain Chem. Eng. 6 (2018) 3754–3764, https://doi.org/10.1021/acssuschemeng.7b04118.

[16] G. Iervolino, I. Tantis, L. Sygellou, V. Vaiano, D. Sannino, P. Lianos, Photocurrent increase by metal modification of Fe_2O_3 photoanodes and its effect on photoelectrocatalytic hydrogen production by degradation of organic substances, Appl. Surf. Sci. 400 (2017) 176–183, https://doi.org/10.1016/j.apsusc.2016.12.173.

[17] D. Raptis, V. Dracopoulos, P. Lianos, Renewable energy production by photoelectrochemical oxidation of organic wastes using WO_3 photoanodes, J. Hazard Mater. 333 (2017) 259–264, https://doi.org/10.1016/j.jhazmat.2017.03.044.

[18] S. Bhattacharjee, V. Andrei, C. Pornrungroj, M. Rahaman, C.M. Pichler, E. Reisner, Reforming of soluble biomass and plastic derived waste using a bias-free Cu30Pd70| Perovskite| Pt photoelectrochemical device, Adv. Funct. Mater. 32 (2022), 2109313, https://doi.org/10.1002/adfm.202109313.

[19] R. Bashiri, N.M. Mohamed, C.F. Kait, S. Sufian, M. Khatani, Enhanced hydrogen production over incorporated Cu and Ni into titania photocatalyst in glycerol-based photoelectrochemical cell: Effect of total metal loading and calcination temperature, Int J. Hydrog. Energy 42 (2017) 9553–9566, https://doi.org/10.1016/j.ijhydene.2017.01.225.

[20] C. Lima, L. Soares, V. Yukuhiro, A. Silva, R. Landers, P. Figueiredo, R. Lima, M. Arruda, C. Longo, C. Pires, P. Fernández, Glycerol (photo)electro-oxidation on carbon supported Ag nanoparticles modified with low amounts of Pt. Activity, Sel. Eff. Visible-Light Irradiat. (2022), https://doi.org/10.26434/CHEMRXIV-2022-B76N2.

[21] N. Perini, C. Hessel, J.L. Bott-Neto, C.T.G.V.M.T. Pires, P.S. Fernandez, E. Sitta, Photoelectrochemical oxidation of glycerol on hematite: thermal effects, in situ FTIR and long-term HPLC product analysis, J. Solid State Electrochem. 25 (2021) 1101–1110, https://doi.org/10.1007/S10008-020-04878-7/METRICS.

[22] Q. Wang, X. Ma, P. Wu, B. Li, L. Zhang, J. Shi, CoNiFe-LDHs decorated Ta3N5 nanotube array photoanode for remarkably enhanced photoelectrochemical glycerol conversion coupled with hydrogen generation, Nano Energy 89 (2021), 106326, https://doi.org/10.1016/j.nanoen.2021.106326.

[23] L.-W. Huang, T.-G. Vo, C.-Y. Chiang, Converting glycerol aqueous solution to hydrogen energy and dihydroxyacetone by the BiVO4 photoelectrochemical cell, Electro Acta 322 (2019), 134725, https://doi.org/10.1016/j.electacta.2019.134725.

[24] D. Liu, J.-C. Liu, W. Cai, J. Ma, H. Bin Yang, H. Xiao, J. Li, Y. Xiong, Y. Huang, B. Liu, Selective photoelectrochemical oxidation of glycerol to high value-added dihydroxyacetone, Nat. Commun. 10 (2019) 1–8, https://doi.org/10.1038/s41467-019-09788-5.

[25] Y.H. Wu, D.A. Kuznetsov, N.C. Pflug, A. Fedorov, C.R. Müller, Solar-driven valorisation of glycerol on $BiVO_4$ photoanodes: effect of co-catalyst and reaction media on reaction selectivity, J. Mater. Chem. A Mater. 9 (2021) 6252–6260, https://doi.org/10.1039/D0TA10480A.

[26] V. Maslova, A. Fasolini, M. Offidani, S. Albonetti, F. Basile, Solar-driven valorization of glycerol towards production of chemicals and hydrogen, Catal. Today 380 (2021) 147–155, https://doi.org/10.1016/j.cattod.2021.03.008.

[27] M. Li, Y. Li, S. Peng, G. Lu, S. Li, Photocatalytic hydrogen generation using glycerol wastewater over Pt/TiO_2, Front. Chem. China 4 (2009) 32–38, https://doi.org/10.1007/s11458-009-0019-6.

[28] P. Ribao, M.A. Esteves, V.R. Fernandes, M.J. Rivero, C.M. Rangel, I. Ortiz, Challenges arising from the use of TiO_2/rGO/Pt photocatalysts to produce hydrogen from crude glycerol compared to synthetic glycerol, Int J. Hydrog. Energy 44 (2019) 28494–28506, https://doi.org/10.1016/j.ijhydene.2018.09.148.

[29] V. Maslova, E.A. Quadrelli, P. Gaval, A. Fasolini, S. Albonetti, F. Basile, Highly-dispersed ultrafine Pt nanoparticles on microemulsion-mediated TiO_2 for production of hydrogen and valuable chemicals via oxidative photo-dehydrogenation of glycerol, J. Environ. Chem. Eng. 9 (2021), 105070, https://doi.org/10.1016/j.jece.2021.105070.

[30] G. Dodekatos, H. Tüysüz, Plasmonic Au/TiO_2 nanostructures for glycerol oxidation, Catal. Sci. Technol. 6 (2016) 7307–7315, https://doi.org/10.1039/C6CY01192F.

[31] L. Guo, Q. Sun, K. Marcus, Y. Hao, J. Deng, K. Bi, Y. Yang, Photocatalytic glycerol oxidation on Au x Cu–CuS@ TiO_2 plasmonic heterostructures, J. Mater. Chem. A Mater. 6 (2018) 22005–22012, https://doi.org/10.1039/C8TA02170H.

[32] Y. Shen, A. Mamakhel, X. Liu, T.W. Hansen, T. Tabanelli, D. Bonincontro, B. B. Iversen, L. Prati, Y. Li, J.W.H. Niemantsverdriet, et al., Promotion mechanisms of Au supported on TiO_2 in thermal-and photocatalytic glycerol conversion, J. Phys. Chem. C. 123 (2019) 19734–19741, https://doi.org/10.1021/acs.jpcc.9b05475.

[33] T. Jedsukontorn, N. Saito, M. Hunsom, Photoinduced glycerol oxidation over plasmonic AU and AuM (M= Pt, Pd and Bi) nanoparticle-decorated TiO_2 photocatalysts, Nanomaterials 8 (2018) 269, https://doi.org/10.3390/nano8040269.

[34] L. Abis, N. Dimitritatos, M. Sankar, S.J. Freakley, G.J. Hutchings, Plasmonic oxidation of glycerol using AuPd/TiO_2 catalysts, Catal. Sci. Technol. 9 (2019) 5686–5691, https://doi.org/10.1039/C9CY01409H.

[35] T.P.A. Ruberu, N.C. Nelson, I.I. Slowing, J. Vela, Selective alcohol dehydrogenation and hydrogenolysis with semiconductor-metal photocatalysts: toward solar-to-chemical energy conversion of biomass-relevant substrates, J. Phys. Chem. Lett. 3 (2012) 2798–2802, https://doi.org/10.1021/jz301309d.

[36] R. Tang, L. Wang, Z. Zhang, W. Yang, H. Xu, A. Kheradmand, Y. Jiang, R. Zheng, J. Huang, Fabrication of MOFs' derivatives assisted perovskite nanocrystal on TiO_2 photoanode for photoelectrochemical glycerol oxidation with simultaneous hydrogen production, Appl. Catal. B 296 (2021), 120382, https://doi.org/10.1016/J.APCATB.2021.120382.

[37] L. Luo, W. Chen, S.M. Xu, J. Yang, M. Li, H. Zhou, M. Xu, M. Shao, X. Kong, Z. Li, H. Duan, Selective Photoelectrocatalytic Glycerol Oxidation to Dihydroxyacetone via Enhanced Middle Hydroxyl Adsorption over a Bi_2O_3-Incorporated Catalyst, J. Am. Chem. Soc. 144 (2022) 7720–7730, https://doi.org/10.1021/jacs.2c00465.

[38] T.G. Vo, C.C. Kao, J.L. Kuo, C. chau Chiu, C.Y. Chiang, Unveiling the crystallographic facet dependence of the photoelectrochemical glycerol oxidation on bismuth vanadate, Appl. Catal. B. 278 (2020), 119303, https://doi.org/10.1016/j.apcatb.2020.119303.

[39] Z. Gu, X. An, R. Liu, L. Xiong, J. Tang, C. Hu, H. Liu, J. Qu, Interface-modulated nanojunction and microfluidic platform for photoelectrocatalytic chemicals upgrading, Appl. Catal. B. 282 (2021), 119541, https://doi.org/10.1016/j.apcatb.2020.119541.

[40] J. Yu, J. González-Cobos, F. Dappozze, F.J. López-Tenllado, J. Hidalgo-Carrillo, A. Marinas, P. Vernoux, A. Caravaca, C. Guillard, WO_3-based materials for photoelectrocatalytic glycerol upgrading into glyceraldehyde: Unravelling the synergistic photo- and electro-catalytic effects, Appl. Catal. B. 318 (2022), 121843, https://doi.org/10.1016/j.apcatb.2022.121843.

[41] C.S. Çetinkaya, G. Khamidov, O.L. Özcan, L. Palmisano, S. Yurdakal, Selective photoelectrocatalytic oxidation of glycerol by nanotube, nanobelt and nanosponge structured TiO_2 on Ti plates, J. Environ. Chem. Eng.10 (2022) 107210, https://doi.org/10.1016/j.jece.2022.107210.

[42] V. Augugliaro, G. Camera-Roda, V. Loddo, G. Palmisano, L. Palmisano, J. Soria, S. Yurdakal, Heterogeneous photocatalysis and photoelectrocatalysis: from unselective abatement of noxious species to selective production of high-value chemicals, J. Phys. Chem. Lett. 6 (2015) 1968–1981, https://doi.org/10.1021/acs.jpclett.5b00294.

[43] V. Malik, S. Srivastava, M.K. Bhatnagar, M. Vishnoi, Comparative study and analysis between Solid Oxide Fuel Cells (SOFC) and Proton Exchange Membrane (PEM) fuel cell–A review, Mater. Today Proc. 47 (2021) 2270–2275, https://doi.org/10.1016/j.matpr.2021.04.203.

[44] G. Cognard, G. Ozouf, C. Beauger, G. Berthomé, D. Riassetto, L. Dubau, R. Chattot, M. Chatenet, F. Maillard, Benefits and limitations of Pt nanoparticles supported on highly porous antimony-doped tin dioxide aerogel as alternative cathode material for proton-exchange membrane fuel cells, Appl. Catal. B. 201 (2017) 381–390, https://doi.org/10.1016/j.apcatb.2016.08.010.

[45] C. Coutanceau, S. Baranton, Electrochemical conversion of alcohols for hydrogen production: a short overview, Wiley Inter. Rev. Energy Environ. 5 (2016) 388–400, https://doi.org/10.1002/wene.193.

[46] A. Rodríguez-Gómez, F. Dorado, P. Sánchez, A.R. de la Osa, Boosting hydrogen and chemicals production through ethanol electro-reforming on Pt-transition metal anodes, J. Energy Chem. 70 (2022) 394–406, https://doi.org/10.1016/j.jechem.2022.02.028.

[47] A. de Lucas-Consuegra, R. Ana, A.B. Calcerrada, J.J. Linares, D. Horwat, A novel sputtered Pd mesh architecture as an advanced electrocatalyst for highly efficient hydrogen production, J. Power Sources 321 (2016) 248–256, https://doi.org/10.1016/j.jpowsour.2016.05.004.

[48] C. Lamy, B. Guenot, M. Cretin, G. Pourcelly, Kinetics analysis of the electrocatalytic oxidation of methanol inside a DMFC working as a PEM electrolysis cell (PEMEC) to generate clean hydrogen, Electro Acta 177 (2015) 352–358, https://doi.org/10.1016/j.electacta.2015.02.069.

[49] F.M. Sapountzi, M.N. Tsampas, H.O.A. Fredriksson, J.M. Gracia, J. W. Niemantsverdriet, Hydrogen from electrochemical reforming of C1–C3 alcohols using proton conducting membranes, Int J. Hydrog. Energy 42 (2017) 10762–10774, https://doi.org/10.1016/j.ijhydene.2017.02.195.

[50] A. Caravaca, F.M. Sapountzi, A. de Lucas-Consuegra, C. Molina-Mora, F. Dorado, J. L. Valverde, Electrochemical reforming of ethanol–water solutions for pure H_2 production in a PEM electrolysis cell, Int J. Hydrog. Energy 37 (2012) 9504–9513, https://doi.org/10.1016/j.ijhydene.2012.03.062.

[51] H.J. Kim, J. Lee, S.K. Green, G.W. Huber, W.B. Kim, Selective glycerol oxidation by electrocatalytic dehydrogenation, ChemSusChem 7 (2014) 1051–1056, https://doi.org/10.1002/cssc.201301218.

[52] A.T. Marshall, R.G. Haverkamp, Production of hydrogen by the electrochemical reforming of glycerol–water solutions in a PEM electrolysis cell, Int J. Hydrog. Energy 33 (2008) 4649–4654, https://doi.org/10.1016/j.ijhydene.2008.05.029.

[53] L. Fan, Y. Ji, G. Wang, J. Chen, K. Chen, X. Liu, Z. Wen, High Entropy Alloy Electrocatalytic Electrode toward Alkaline Glycerol Valorization Coupling with Acidic Hydrogen Production, J. Am. Chem. Soc. 144 (2022) 7224–7235, https://doi.org/10.1021/jacs.1c13740.

[54] J. De Paula, D. Nascimento, J.J.L. Leon, Electrochemical reforming of glycerol in alkaline PBI-based PEM reactor for hydrogen production, Chem. Eng. Trans. 41 (2014) 205–210, https://doi.org/10.3303/CET1441035.

[55] J. de Paula, D. Nascimento, J.J. Linares, Influence of the anolyte feed conditions on the performance of an alkaline glycerol electroreforming reactor, J. Appl. Electrochem 45 (2015) 689–700, https://doi.org/10.1007/s10800-015-0848-6.

[56] V. Bambagioni, M. Bevilacqua, C. Bianchini, J. Filippi, A. Lavacchi, A. Marchionni, F. Vizza, P.K. Shen, Self-sustainable production of hydrogen, chemicals, and energy from renewable alcohols by electrocatalysis, ChemSusChem 3 (2010) 851–855, https://doi.org/10.1007/s10800-015-0848-6.

[57] D.M. Morales, D. Jambrec, M.A. Kazakova, M. Braun, N. Sikdar, A. Koul, A.C. Brix, S. Seisel, C. Andronescu, W. Schuhmann, Electrocatalytic conversion of glycerol to oxalate on Ni oxide nanoparticles-modified oxidized multiwalled carbon nanotubes, ACS Catal. 12 (2022) 982–992, https://doi.org/10.1021/acscatal.1c04150.

[58] A.C. Brix, D.M. Morales, M. Braun, D. Jambrec, J.R.C. Junqueira, S. Cychy, S. Seisel, J. Masa, M. Muhler, C. Andronescu, et al., Electrocatalytic Oxidation of Glycerol Using Solid-State Synthesised Nickel Boride: Impact of Key Electrolysis Parameters on Product Selectivity, ChemElectroChem 8 (2021) 2336–2342, https://doi.org/10.1002/celc.202100739.

[59] A.C. Brix, M. Dreyer, A. Koul, M. Krebs, A. Rabe, U. Hagemann, S. Varhade, C. Andronescu, M. Behrens, W. Schuhmann, et al., Structure-Performance Relationship of LaFe1-xCoxO3 Electrocatalysts for Oxygen Evolution, Isopropanol Oxidation, and Glycerol Oxidation, ChemElectroChem 9 (2022), e202200092, https://doi.org/10.1002/celc.202200092.

[60] Y. Zhang, H. Hu, W. Kang, G. Qiu, R. Liang, L. Deng, H. Yuan, Enhancing hydrogen evolution by photoelectrocatalysis of water splitting over a CdS flowers-loaded TiO_2 nanotube array film on the Ti foil substrate, Ceram. Int 46 (2020) 17606–17613, https://doi.org/10.1016/J.CERAMINT.2020.04.062.

[61] Y. Li, H. Yu, C. Zhang, W. Song, G. Li, Z. Shao, B. Yi, Effect of water and annealing temperature of anodized TiO_2 nanotubes on hydrogen production in photoelectrochemical cell, Electro Acta 107 (2013) 313–319, https://doi.org/10.1016/J.ELECTACTA.2013.05.090.

[62] R. Marschall, C. Klaysom, A. Mukherji, M. Wark, G.Q. Lu, L. Wang, Composite proton-conducting polymer membranes for clean hydrogen production with solar light in a simple photoelectrochemical compartment cell, Int J. Hydrog. Energy 37 (2012) 4012–4017, https://doi.org/10.1016/J.IJHYDENE.2011.11.097.

[63] T. Stoll, G. Zafeiropoulos, M.N. Tsampas, Solar fuel production in a novel polymeric electrolyte membrane photoelectrochemical (PEM-PEC) cell with a web of titania nanotube arrays as photoanode and gaseous reactants, Int J. Hydrog. Energy 41 (2016) 17807–17817, https://doi.org/10.1016/J.IJHYDENE.2016.07.230.

[64] X. Kang, L. Chaperman, A. Galeckas, S. Ammar, F. Mammeri, T. Norby, A. Chatzitakis, Water Vapor Photoelectrolysis in a Solid-State Photoelectrochemical Cell with TiO_2 Nanotubes Loaded with CdS and CdSe Nanoparticles, ACS Appl. Mater. Interfaces 13 (2021) 46875–46885, https://doi.org/10.1021/acsami.1c13047.

[65] F. Amano, A. Shintani, H. Mukohara, Y.M. Hwang, K. Tsurui, Photoelectrochemical gas-electrolyte-solid phase boundary for hydrogen production from water vapor, Front Chem. 6 (2018) 598, https://doi.org/10.3389/FCHEM.2018.00598/BIBTEX.

[66] J. Yu, F. Dappozze, J. Martín-Gomez, J. Hidalgo-Carrillo, A. Marinas, P. Vernoux, A. Caravaca, C. Guillard, Glyceraldehyde production by photocatalytic oxidation of glycerol on WO_3-based materials, Appl. Catal. B. 299 (2021), 120616, https://doi.org/10.1016/j.apcatb.2021.120616.

[67] Y.-W. Chen, Y.-H. Hsu, Effects of reaction temperature on the photocatalytic activity of TiO2 with Pd and Cu cocatalysts, Catalysts 11 (2021) 966, https://doi.org/10.3390/catal11080966.

[68] M. Umar, H.A. Aziz, Photocatalytic degradation of organic pollutants in water, Organic Pollutants-Monitoring, Risk Treat. 8 (2013) 196–197, https://doi.org/10.5772/53699.

[69] A. Gomis-Berenguer, J. Iniesta, D.J. Fermín, C.O. Ania, Photoelectrochemical response of WO_3/nanoporous carbon anodes for photocatalytic water oxidation, C. (Basel) 4 (2018) 45, https://doi.org/10.3390/c4030045.

[70] M. Ibadurrohman, K. Hellgardt, Photoelectrochemical performance of graphene-modified TiO_2 photoanodes in the presence of glycerol as a hole scavenger, Int J. Hydrog. Energy 39 (2014) 18204–18215, https://doi.org/10.1016/j.ijhydene.2014.08.142.

[71] F.K. Chong, E. Nurlaela, B.K. Dutta, Impact of glycerol as scavenger for solar hydrogen production from water, Int. J. Energy Environ. 8 (2014) 19–26.

[72] K.K. Upadhyay, M. Altomare, S. Eugénio, P. Schmuki, T.M. Silva, M.F. Montemor, On the supercapacitive behaviour of anodic porous WO_3-based negative electrodes, Electro Acta 232 (2017) 192–201, https://doi.org/10.1016/j.electacta.2017.02.131.

[73] S.P. Gupta, H.H. Nishad, S.D. Chakane, S.W. Gosavi, D.J. Late, P.S. Walke, Phase transformation in tungsten oxide nanoplates as a function of post-annealing temperature and its electrochemical influence on energy storage, Nanoscale Adv. 2 (2020) 4689–4701, https://doi.org/10.1039/D0NA00423E.

[74] S. Sfaelou, L.-C. Pop, O. Monfort, V. Dracopoulos, P. Lianos, Mesoporous WO_3 photoanodes for hydrogen production by water splitting and PhotoFuelCell operation, Int J. Hydrog. Energy 41 (2016) 5902–5907, https://doi.org/10.1016/j.ijhydene.2016.02.063.

[75] J.C. Grenier, A. Wattiaux, J.P. Doumerc, P. Dordor, L. Fournes, J.P. Chaminade, M. Pouchard, Electrochemical oxygen intercalation into oxide networks, J. Solid State Chem. 96 (1992) 20–30, https://doi.org/10.1016/S0022-4596(05)80293-2.

[76] H. Liang, Z. Cao, C. Xia, F. Ming, W. Zhang, A.-H. Emwas, L. Cavallo, H. N. Alshareef, Tungsten blue oxide as a reusable electrocatalyst for acidic water oxidation by plasma-induced vacancy engineering, CCS Chem. 3 (2021) 1553–1561, https://doi.org/10.31635/ccschem.020.202000325.

[77] J. González-Cobos, S. Baranton, C. Coutanceau, Development of bismuth-modified PtPd nanocatalysts for the electrochemical reforming of polyols into hydrogen and value-added chemicals, ChemElectroChem 3 (2016) 1694–1704, https://doi.org/10.1002/celc.201600147.

[78] M.S.E. Houache, R. Safari, U.O. Nwabara, T. Rafaïdeen, G.A. Botton, P.J.A. Kenis, S. Baranton, C. Coutanceau, E.A. Baranova, Selective Electrooxidation of Glycerol to Formic Acid over Carbon Supported Ni1–x M x (M= Bi, Pd, and Au) Nanocatalysts and Coelectrolysis of CO_2, ACS Appl. Energy Mater. 3 (2020) 8725–8738, https://doi.org/10.1021/acsaem.0c01282.

[79] M.S.E. Houache, A. Shubair, M.G. Sandoval, R. Safari, G.A. Botton, P.V. Jasen, E. A. González, E.A. Baranova, Influence of Pd and Au on electrochemical valorization of glycerol over Ni-rich surfaces, J. Catal. 396 (2021) 1–13, https://doi.org/10.1016/j.jcat.2021.02.008.

[80] M.S.E. Houache, K. Hughes, R. Safari, G.A. Botton, E.A. Baranova, Modification of nickel surfaces by bismuth: Effect on electrochemical activity and selectivity toward glycerol, ACS Appl. Mater. Interfaces 12 (2020) 15095–15107, https://doi.org/10.1021/acsami.9b22378.

[81] A. Shubair, M.S.E. Houache, S.S. Mousavi M, G.A. Botton, E.A. Baranova, Electrolysis of glycerol to value-added chemicals in alkaline media, J. Chem. Technol. Biotechnol. 97 (2022) 1950–1958, https://doi.org/10.1002/jctb.7088.

[82] D. Katakis, C. Mitsopoulou, E. Vrachnou, Photocatalytic splitting of water: increase in conversion and energy storage efficiency, J. Photochem. Photobio. A Chem. 81 (1994) 103–106, https://doi.org/10.1016/1010-6030(94)03777-9.

[83] J.J. Velázquez, R. Fernández-González, L. Díaz, E.P. Melián, V.D. Rodríguez, P. Núñez, Effect of reaction temperature and sacrificial agent on the photocatalytic H_2-production of Pt-TiO_2, J. Alloy. Compd. 721 (2017) 405–410, https://doi.org/10.1016/j.jallcom.2017.05.314.

[84] Z. Ghasemi, H. Younesi, A.A. Zinatizadeh, Kinetics and thermodynamics of photocatalytic degradation of organic pollutants in petroleum refinery wastewater over nano-TiO_2 supported on Fe-ZSM-5, J. Taiwan Inst. Chem. Eng. 65 (2016) 357–366, https://doi.org/10.1016/j.jtice.2016.05.039.

[85] Q. Hu, B. Liu, M. Song, X. Zhao, Temperature effect on the photocatalytic degradation of methyl orange under UV–vis light irradiation (others), J. Wuhan. Univ. Technol. -Mater. Sci. Ed. 25 (2010) 210–213, https://doi.org/10.1007/s11595-010-2210-5.

[86] J.-M. Herrmann, Heterogeneous photocatalysis: fundamentals and applications to the removal of various types of aqueous pollutants, Catal. Today 53 (1999) 115–129, https://doi.org/10.1016/S0920-5861(99)00107-8.

[87] Y. Xue, Y. Wang, Z. Pan, K. Sayama, Electrochemical and photoelectrochemical water oxidation for hydrogen peroxide production, Angew. Chem. Int. Ed. 60 (2021) 10469–10480, https://doi.org/10.1002/anie.202011215.

[88] K. Zhang, J. Liu, L. Wang, B. Jin, X. Yang, S. Zhang, J.H. Park, Near-complete suppression of oxygen evolution for photoelectrochemical H_2O oxidative H_2O_2

synthesis, J. Am. Chem. Soc. 142 (2020) 8641–8648, https://doi.org/10.1021/jacs.9b13410.
[89] G. Dodekatos, S. Schünemann, H. Tüysüz, Recent advances in thermo-, photo-, and electrocatalytic glycerol oxidation, ACS Catal. 8 (2018) 6301–6333, https://doi.org/10.1021/acscatal.8b01317.
[90] J.E. Carrera-Crespo, I. Fuentes-Camargo, R.E. Palma-Goyes, U.M. García-Pérez, J. Vazquez-Arenas, I. Chairez, T. Poznyak, Unrevealing the effect of transparent fluorine-doped tin oxide (FTO) substrate and irradiance configuration to unmask the activity of FTO-$BiVO_4$ heterojunction, Mater. Sci. Semicond. Process 128 (2021), 105717, https://doi.org/10.1016/j.mssp.2021.105717.